Engineering Structures 275 (2023) 114924

Contents lists available at ScienceDirect

Engineering Structures

journal homepage: www.elsevier.com/locate/engstruct

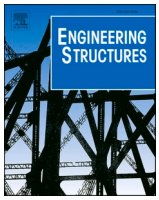

Review article

The Continuous Strength Method – Review and outlook

Leroy Gardner [a,*], Xiang Yun [b], Fiona Walport [a]

[a] Department of Civil and Environmental Engineering, Imperial College London, London SW7 2AZ, UK
[b] Department of Civil and Structural Engineering, University of Sheffield, Sheffield S1 3JD, UK

ARTICLE INFO

Keywords:
Composite
Continuous Strength Method
Deformation based
Design
Design by advanced analysis
Elevated temperature
Local buckling
Stainless steel
Steel

ABSTRACT

The Continuous Strength Method (CSM) is a deformation-based approach to the design of structures that enables a continuous, rational and accurate allowance for material nonlinearity (i.e. the spread of plasticity and strain hardening). Central to the method is the application of strain limits, determined on the basis of the local slenderness of full cross-sections, to define the resistance of a structural member or system. The method can be applied to structures formed using different materials (e.g. steel, stainless steel or aluminium) and manufacturing processes (e.g. hot-rolled or cold-formed) through the assignment of suitable stress–strain relationships, and can be used for steel–concrete composite design and in fire scenarios. In composite construction, the CSM enables a more rigorous assessment to be made of the development of strength in the structural system taking due account of compatibility between the constituent materials. The design method enables enhancements in structural efficiency and, unlike traditional approaches, allows the assessment of both strength and ductility (which is particularly relevant for high strength steel) demands at the ultimate limit state. For hand calculations, a set of straightforward CSM design equations have been developed. Recognising the increasing importance and use of advanced analysis (i.e. GMNIA), recent research, summarised herein, has focussed on integration of the CSM strain limits into a framework of design by second order inelastic analysis, where the benefits of the method become even more substantial. This paper provides a review of the background and recent developments to the CSM, including incorporation into design standards. Current and ongoing research to expand the scope of the CSM is summarised and recommendations for future work are also set out.

1. Introduction

The origins of the Continuous Strength Method (CSM) date back to 2002 [1], where the deformation-based design concept was developed and applied to structural stainless steel elements. In 2008, the name 'Continuous Strength Method' [2] was first introduced to reflect the continuity in resistance predictions with varying cross-section slenderness, in contrast to the step-wise resistance predictions associated with traditional strength-based design, built upon the cross-section classification concept. At first, the perceived benefits of the CSM were limited merely to improved cross-section capacity predictions, particularly for materials with rounded stress–strain curves and a high degree of strain hardening. Later, further developments highlighted the breadth of applicability of the method and its true potential as a system-level design approach. The CSM has now been applied to the design of steel [3–6], stainless steel [7–12], aluminium alloy [13–15], reinforced concrete [16,17] and composite structures [18–21], as well as steel structures in fire [22,23]. Recent attention has been focussed upon extension of the CSM to member-level design [24–28] and incorporation of the CSM into a framework of design by advanced analysis (i.e. GMNIA) [29–34] and into codes of practice; the CSM now features in the AISC Design Guide for Structural Stainless Steel (2013) [35], the Fourth Edition of the SCI Design Manual for Structural Stainless Steel (2017) [36], the draft European Standard prEN 1993–1-4 [37] for the design of stainless steel structures, the draft European Standard prEN 1993–1-14 [38] for the design of steel structures by finite element analysis, the ASCE Specification ASCE-8–21 [39] for the design of cold-formed stainless steel structures and the AISC Specification AISC 370 [40] for the design of hot-rolled and welded stainless steel structures.

A review of the background, key concepts and components, and fundamental design equations of the CSM is presented in this paper. Current and ongoing research to expand the scope and range of applicability of the CSM is summarised. Finally, recommendations for future work on CSM development are set out to provide insight into what aspects need to be explored further and to encourage research to take place in these areas.

* Corresponding author.

https://doi.org/10.1016/j.engstruct.2022.114924
Received 6 June 2022; Received in revised form 21 July 2022; Accepted 29 August 2022
Available online 22 November 2022

2. Background and CSM key components

2.1. Background

The CSM has two key components: (1) a 'base curve' that defines the limiting strain ε_{csm} for a cross-section (i.e. the deformation capacity) based on its local slenderness and (2) a constitutive model that provides a suitable representation of the stress–strain relationship of the material. The CSM is a ground-up design approach that starts from the analysis of cross-sections, but extends to the design of members and frames. The two key components of the CSM are described in the following two sub-sections of the paper.

2.2. Deformation capacity (strain limits)

2.2.1. General

Since the Continuous Strength Method is a deformation-based design approach, it requires the determination of a relationship between the maximum limiting strain that a cross-section can endure prior to reaching its ultimate capacity and its local slenderness. This relationship is equivalent to the process of cross-section classification used in many structural metallic design codes, but instead of placing a cross-section into a discrete behavioural class, a normalised limiting strain is assigned. For slender cross-sections, the limiting strain is below the yield strain and there is therefore no benefit in capacity to be gained from the spread of plasticity and strain hardening, except in the case of non-doubly-symmetric cross-sections that can have limiting strains on the compression side less than the yield strain yet experience plasticity and strain hardening on the tensile side. For non-slender cross-sections, the limiting strain is beyond the yield strain and capacity benefits can be derived from the spread of plasticity and strain hardening. The base curve for cross-sections comprising flat plates (e.g. I-sections and rectangular hollow sections) are described in Section 2.2.2, while circular hollow sections (CHS) are considered in Section 2.2.3.

2.2.2. Base curve – Plated cross-sections

At the core of the CSM is a base curve, which defines a continuous relationship between the deformation capacity of a cross-section and its cross-section slenderness $\bar{\lambda}_p$. The cross-section slenderness is defined by $\bar{\lambda}_p = \sqrt{f_y/\sigma_{cr}}$, where f_y is the yield strength (or 0.2% proof stress in the case of materials with rounded stress–strain curves) and σ_{cr} is the elastic local buckling stress of the full cross-section. While in traditional design, local buckling is generally treated on an element-by-element basis through cross-section classification and effective width formulae, in reality, a cross-section is an assemblage of plates that interact with one another. It is, therefore, more appropriate to consider local buckling on a full cross-section basis. The CSM is very much an ally of the Direct Strength Method (DSM) [41,42] in this regard, in the sense that the susceptibility of cross-sections to local buckling is considered on this full cross-section basis, allowing for element interaction; the elastic local buckling stress σ_{cr} may be determined for the full cross-section either using numerical methods, such as the finite strip software CUFSM [43], or approximate analytical formulae [44,45].

The CSM deformation capacity is defined through the strain ratio $\varepsilon_{csm}/\varepsilon_y$, as given by Eqs. (1) and (2) for non-slender and slender cross-sections, respectively,

$$\frac{\varepsilon_{csm}}{\varepsilon_y} = \frac{0.25}{\bar{\lambda}_p^{3.6}}, \text{ but } \frac{\varepsilon_{csm}}{\varepsilon_y} \leqslant \min\left(\Omega, \frac{C_1\varepsilon_u}{\varepsilon_y}\right) \text{ for } \bar{\lambda}_p \leqslant 0.68 \quad (1)$$

$$\frac{\varepsilon_{csm}}{\varepsilon_y} = \left(1 - \frac{0.222}{\bar{\lambda}_p^{1.05}}\right)\frac{1}{\bar{\lambda}_p^{1.05}} \text{ for } 0.68 < \bar{\lambda}_p \leqslant 1.60 \quad (2)$$

where ε_{csm} is the maximum strain that a cross-section can resist prior to failure and ε_y is the material yield strain equal to f_y/E with E being the Young's modulus. In Eq. (1), two upper bounds are placed on the CSM strain ratio $\varepsilon_{csm}/\varepsilon_y$; the first limit of Ω defines the maximum tolerable level of plastic strains and may be defined on a project by project basis, with a recommended value of 15, and the second limit of $C_1\varepsilon_u/\varepsilon_y$, where C_1 is a coefficient corresponding to the adopted CSM material model as described in Section 2.3.2 and ε_u is the strain at the material ultimate tensile strength f_u, defines a 'cut-off' strain to avoid over-predictions of material strength when using the resistance functions developed for hand calculations, which are outlined in Section 3. Both Eqs. (1) and (2) pass through the identified transition point, i.e. (0.68, 1), ensuring compatibility between the CSM base curves for non-slender and slender cross-sections. The transition between slender and non-slender plated cross-sections occurs at $\bar{\lambda}_p = 0.68$ [7]. At this slenderness, cross-sections fail at the yield load N_y (i.e. determined as the product of the gross cross-sectional area A and the material yield strength f_y) in compression and the elastic moment M_{el} (for symmetric sections) in bending. Below this limit (i.e. for non-slender cross-sections with $\bar{\lambda}_p \leqslant 0.68$), failure occurs beyond the yield strain and benefit can be taken from the spread of plasticity and potentially strain hardening. Beyond this limit (i.e. for slender cross-sections with $\bar{\lambda}_p > 0.68$), failure occurs below the yield strain.

A detailed description of the establishment of the CSM base curve is presented in [2,7,46,47], while the underpinning experimental data are shown in Figs. 1 and 2 for non-slender and slender cross-sections, respectively. The collected test data include results for hot-rolled and cold-formed steel, stainless steel and aluminium stub columns (in which ε_{csm} was determined based on average axial shortening at ultimate load) and beams in four-point bending (in which ε_{csm} was determined based on average curvature in the uniform moment region at ultimate load). The base curve for non-slender cross-sections ($\bar{\lambda}_p \leqslant 0.68$) was fitted to the test data (see Fig. 1), with a single curve (Eq. (1)) applicable to all metallic materials, despite the variation in mechanical properties and strain hardening characteristics. This response would not necessarily be expected based on tangent modulus theory and consideration only of elastic critical buckling, but may be explained with reference to the metallurgical process of yielding, characterised by the occurrence of a series of localised jumps in strain (i.e. slip movements) rather than uniform deformation [48], and to the influence of (inelastic) post-buckling, where there is a dependency on both the strain hardening slope and absolute material strength reserves beyond yield [49,50]. The form of the base curve for slender cross-sections ($\bar{\lambda}_p > 0.68$) (Eq. (2)) is the same as the strength curves used in the effective width method of EN 1993–1-5 [51] (also plotted in Fig. 2) and the DSM [41,42].

For structural fire design, higher deformations are expected, and indeed tolerated, than at room temperature. Extension of the CSM to the

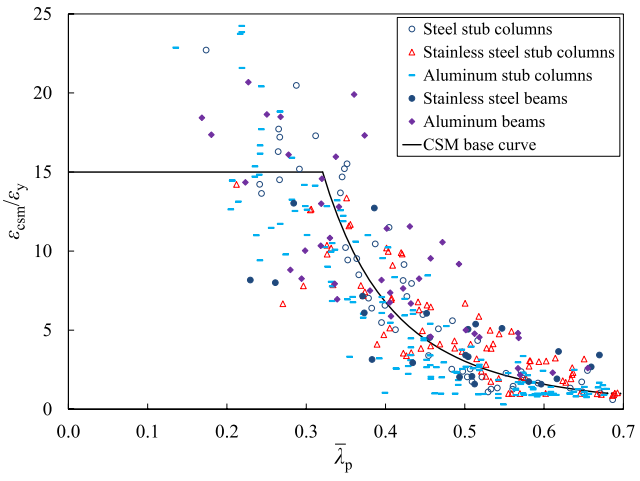

Fig. 1. Base curve – relationship between strain ratio and slenderness for non-slender cross-sections.

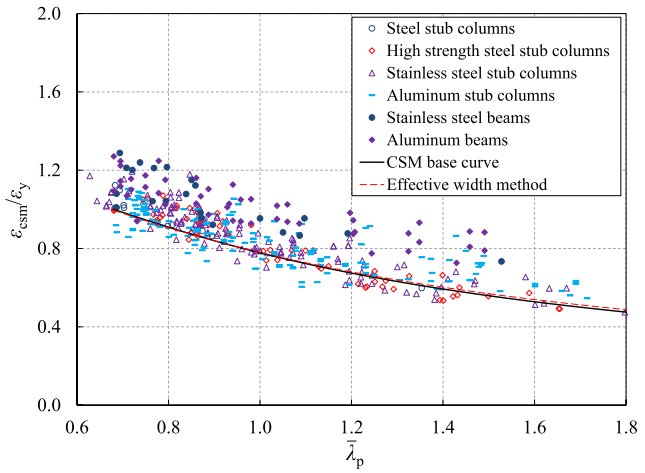

Fig. 2. Base curve – relationship between strain ratio and slenderness for slender cross-sections.

design of cross-sections at elevated temperature has been investigated by Theofanous et al. [22] and Yun et al. [23]. It was found that the base curve at room temperature (Eq. (2)) was also applicable at elevated temperatures, provided due account was taken of the reduction in strength and Young's modulus of the material in the determination of cross-section slenderness. The CSM was shown to offer improved predictions of element capacity in fire over existing design methods.

2.2.3. Base curve - circular hollow sections

The base curve defining the relationship between deformation capacity and local slenderness $\bar{\lambda}_c$ for non-slender and slender circular hollow sections (CHS) was developed in [2,52–54]. The base curve established in [53] is included in prEN 1993–1-4 [37] and given by:

$$\frac{\varepsilon_{csm}}{\varepsilon_y} = \frac{4.44 \times 10^{-3}}{\bar{\lambda}_c^{4.5}}, \text{ but } \frac{\varepsilon_{csm}}{\varepsilon_y} \leqslant \min\left(\Omega, \frac{C_1 \varepsilon_u}{\varepsilon_y}\right) \text{ for } \bar{\lambda}_c \leqslant 0.3 \tag{3}$$

$$\frac{\varepsilon_{csm}}{\varepsilon_y} = \left(1 - \frac{0.224}{\bar{\lambda}_c^{0.342}}\right) \frac{1}{\bar{\lambda}_c^{0.342}} \text{ for } 0.3 < \bar{\lambda}_c \leqslant 0.6 \tag{4}$$

where

$$\bar{\lambda}_c = \sqrt{f_y / \sigma_{cr,c}} \tag{5}$$

with the elastic buckling stress $\sigma_{cr,c}$ of a CHS under compression, bending or combined loading being determined from the classical expression of Eq. (6) [55], with further discussion given in [56]:

$$\sigma_{cr,c} = \frac{E}{\sqrt{3(1-\nu^2)}} \frac{2t}{D} \tag{6}$$

where t is the thickness of the CHS, D is the outer diameter of the CHS and ν is the Poisson's ratio.

A revised base curve for CHS and elliptical hollow sections (EHS) [57] was developed by Meng et al. [54], as given by Eqs. (7) and (8), to account for the different deformation capacities under different loading scenarios:

$$\frac{\varepsilon_{csm}}{\varepsilon_y} = \left(\frac{\bar{\lambda}_0}{\bar{\lambda}_c}\right)^B, \text{ but } \frac{\varepsilon_{csm}}{\varepsilon_y} \leqslant \min\left(\Omega, \frac{C_1 \varepsilon_u}{\varepsilon_y}\right) \text{ for } \bar{\lambda}_c \leqslant \bar{\lambda}_0 \tag{7}$$

$$\frac{\varepsilon_{csm}}{\varepsilon_y} = \left(1 - \frac{A}{\bar{\lambda}_c^{0.3}}\right) \frac{1}{\bar{\lambda}_c^{0.3}} \text{ for } \bar{\lambda}_0 < \bar{\lambda}_c \leqslant 0.6 \tag{8}$$

where $\bar{\lambda}_0$ is the slenderness limit between non-slender and slender CHS and EHS, and A and B are coefficients that describe the shape of the base curve; $\bar{\lambda}_0$, A and B are all expressed in terms of a parameter ψ, as given by Eqs. (9)-(11), respectively.

$$\bar{\lambda}_0 = 0.43 - 0.07((1+\psi)/2)^2 \tag{9}$$

$$A = \left(1 - \bar{\lambda}_0^{0.3}\right)\bar{\lambda}_0^{0.3} \tag{10}$$

$$B = 2.5 + ((1+\psi)/2)^2 \tag{11}$$

The parameter ψ describes the ratio between compression and bending for CHS and EHS and is defined by Eq. (12), where N_{Ed} is the design compression load, $M_{y,Ed}$ and $M_{z,Ed}$ are the design bending moments about the major and minor axis, respectively, and $M_{el,y}$ and $M_{el,z}$ are the elastic bending moment capacities about the major and minor axis, respectively.

$$\psi = \frac{\frac{N_{Ed}}{N_y} - \frac{M_{y,Ed}}{M_{el,y}} - \frac{M_{z,Ed}}{M_{el,z}}}{\frac{N_{Ed}}{N_y} + \frac{M_{y,Ed}}{M_{el,y}} + \frac{M_{z,Ed}}{M_{el,z}}} \tag{12}$$

Both base curves, alongside the collected test data, are plotted in Fig. 3, where N denotes cross-sectional tests in compression (i.e. stub column tests) and M denotes cross-sectional tests in bending (beam tests). The newer base curve [54] can be seen from Fig. 3 to capture the trend of the test data more accurately, and is included in ASCE-8–21 [39]. There are, however, some test data points that deviate noticeably from the trend of the base curve; this may be attributed to the sensitivity of the cross-sectional behaviour of CHS to initial local imperfections and loading eccentricities.

2.3. Material models

2.3.1. General

Early versions of the CSM adopted the compound Ramberg–Osgood model, which can accurately capture the stress–strain response of stainless steels, but results in relatively complex resistance equations that are inconvenient for hand calculations. Thus, simplified material models have been developed and employed throughout the recent development of the CSM; the material models used in the CSM resistance functions suitable for hand calculations are described in Section 2.3.2. For design by second order inelastic analysis, as described in Section 5, where internal forces and moments are determined within the analysis by numerical integration, more accurate and complex material stress–-strain models can be easily accommodated; the material models for the design of structures by finite element (FE) analysis are introduced in Section 2.3.3.

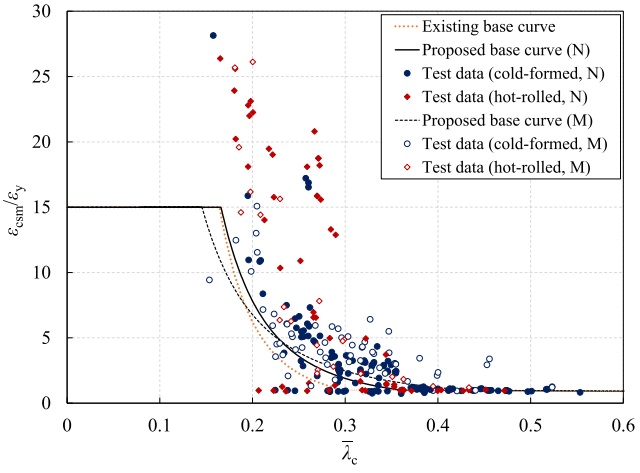

Fig. 3. Base curve – relationship between strain ratio and slenderness for slender and non-slender CHS and EHS.

2.3.2. Material models for simplified resistance functions

To facilitate hand calculations, relatively simple resistance functions are required. A quad-linear material model has been established by Yun and Gardner [58], to accurately represent the elastic, yield plateau and strain hardening characteristics of hot-rolled steels, while a bilinear (i.e. elastic, linear hardening) material model has been developed to represent the strain hardening behaviour of metallic materials with a rounded stress–strain response, such as cold-formed steels [59], austenitic and duplex stainless steels [7], ferritic stainless steels [60] and aluminium alloys [13].

The quad-linear material model [58] for hot-rolled steels is illustrated in Fig. 4 and described by Eq. (13). In Eq. (13), σ and ε are engineering stress and strain, respectively, ε_{sh} is the strain hardening strain at which the plastic yield plateau ends and strain hardening initiates and E_{sh} is the slope of the first linear hardening region determined as the slope of the line passing through two defined points on the stress–strain curve (see Fig. 4): the strain hardening point (ε_{sh}, f_y) and a specified maximum point ($C_2\varepsilon_u$, f_u). Two coefficients are employed in the quad-linear material model: C_1 defines the transition point between the first and second strain hardening regions and is also included in the CSM base curves for non-slender cross-sections (Eqs. (1), (3) and (7)) to avoid over-predictions of strength for the adopted resistance functions, and C_2 is used to define E_{sh} in Eq. (14). Predictive expressions for the strain hardening strain ε_{sh} and the material coefficients of C_1 and C_2 are given by Eqs. (15)-(17), respectively.

$$\sigma = \begin{cases} E\varepsilon & \text{for } \varepsilon \leqslant \varepsilon_y \\ f_y & \text{for } \varepsilon_y < \varepsilon \leqslant \varepsilon_{sh} \\ f_y + E_{sh}(\varepsilon - \varepsilon_{sh}) & \text{for } \varepsilon_{sh} < \varepsilon \leqslant C_1\varepsilon_u \\ f_{C_1\varepsilon_u} + \dfrac{f_u - f_{C_1\varepsilon_u}}{\varepsilon_u - C_1\varepsilon_u}(\varepsilon - C_1\varepsilon_u) & \text{for } C_1\varepsilon_u < \varepsilon \leqslant \varepsilon_u \end{cases} \tag{13}$$

$$E_{sh} = \frac{f_u - f_y}{C_2\varepsilon_u - \varepsilon_{sh}} \quad \text{for hot-rolled carbon steels} \tag{14}$$

$$\varepsilon_{sh} = 0.1\frac{f_y}{f_u} - 0.055, \quad \text{but } 0.015 \leqslant \varepsilon_{sh} \leqslant 0.03 \tag{15}$$

$$C_1 = \frac{\varepsilon_{sh} + 0.25(\varepsilon_u - \varepsilon_{sh})}{\varepsilon_u} \tag{16}$$

$$C_2 = \frac{\varepsilon_{sh} + 0.4(\varepsilon_u - \varepsilon_{sh})}{\varepsilon_u} \tag{17}$$

The bilinear (i.e. elastic, linear hardening) constitutive model for metallic materials characterised by a rounded stress–strain response with no sharply defined yield point, such as cold-formed steels, stainless steels and aluminium alloys, is illustrated in Fig. 5 and described by Eq. (18). As shown in Fig. 5, the bilinear material model effectively starts at the 0.2% off-set plastic strain, and assumes elastic stress–strain

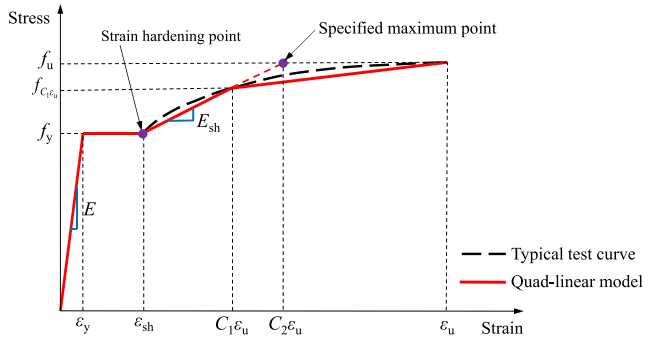

Fig. 4. Typical test stress–strain curve and quad-linear material model for hot-rolled steels.

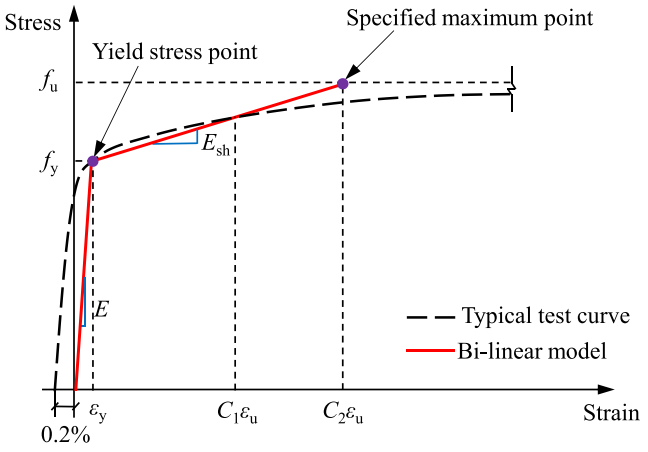

Fig. 5. Typical test stress–strain curve and bilinear (i.e. elastic, linear hardening) constitutive model for materials with a rounded stress–strain response.

behaviour up to the yield (i.e. 0.2% proof) strength f_y. The slope of the elastic region is taken as the Young's modulus E. Note that the material nonlinearity in this region has been accounted for by subtracting 0.2% plastic strain from the defined deformation capacity in the development of the base curve [2,7,46,47]. Similar to the quad-linear material model, the slope of the linear hardening region E_{sh} of the bi-linear model is determined as the slope of the line passing through two defined points on the stress–strain curve (see Fig. 5): the yield point (ε_y, f_y) and a specified maximum point ($C_2\varepsilon_u$, f_u).

To reflect the differing strain hardening characteristics of different materials, the slope of the linear hardening region E_{sh} of the bilinear material model is determined with reference to the material coefficients C_i from Eq. (19) given in Table 1. The strain hardening slope is a function of f_y, f_u and ε_y, all of which are readily available to a designer, as well as ε_u, which is not typically available to a designer as it is not supplied in material specifications, but may be predicted using Eq. (20). Detailed information on the derivation of these material coefficients is given by Yun et al. [59] and Gardner and Yun [61] for cold-formed steels, Afshan and Gardner [7], Bock et al. [60] and Arrayago et al. [62] for stainless steels, and Su et al. [13,14] and Yun et al. [63] for aluminium alloys.

$$\sigma = \begin{cases} E\varepsilon & \text{for } \varepsilon < \varepsilon_y \\ f_y + E_{sh}(\varepsilon - \varepsilon_y) & \text{for } \varepsilon_y \leqslant \varepsilon \leqslant C_2\varepsilon_u \end{cases} \tag{18}$$

$$E_{sh} = \frac{f_u - f_y}{C_2\varepsilon_u - \varepsilon_y} \tag{19}$$

$$\varepsilon_u = C_3\left(1 - \frac{f_y}{f_u}\right) + C_4, \quad \text{but } \varepsilon_u \geqslant 0.06 \text{ for hot-rolled steels} \tag{20}$$

The bilinear material model is able to capture the essence of the strain hardening behaviour to a suitably accurate degree for significantly improved strength predictions within the CSM design framework. The greatest benefit from strain hardening is derived for those materials that exhibit the highest strain hardening slopes (particularly the austenitic and duplex stainless steels), though worthwhile capacity advantages are achieved for all materials.

Table 1
Summary of coefficients for the CSM elastic, linear hardening material model.

Type of material	C_1	C_2	C_3	C_4
Hot-rolled steels	Eq. (16)	Eq. (17)	0.60	0
Cold-formed steels	0.40	0.45	0.60	0
Austenitic and duplex stainless steels	0.10	0.16	1.00	0
Ferritic stainless steels	0.40	0.45	0.60	0
Aluminium alloys	0.50	0.50	0.13	0.06

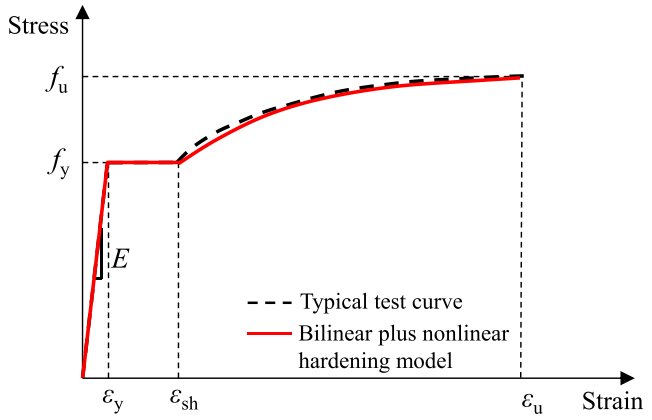

Fig. 6. Typical test stress–strain curve and bilinear plus nonlinear hardening model for hot-rolled steels.

2.3.3. Material models for design by finite element analysis

In design by finite element analysis, member stability checks are typically circumvented, and resistances are directly dependent on the adopted material model. It is therefore crucial that the stress–strain properties are accurately represented. For hot-rolled steels, either the quad-linear material model (introduced in Section 2.3.2) or a bilinear plus nonlinear hardening model may be used. The former features in prEN 1993–1-14 [38] for the design of steel structures using finite element analysis, while the latter was proposed by Yun and Gardner [58] as an alternative to the quad-linear model to capture the rounded strain hardening response after the yield plateau more smoothly, as shown in Fig. 6 and expressed by Eq. (21), where ε_{sh} and ε_u are calculated from the Eq. (15) and (20), respectively.

$$\sigma = \begin{cases} E\varepsilon & \text{for } \varepsilon \leqslant \varepsilon_y \\ f_y & \text{for } \varepsilon_y \leqslant \varepsilon \leqslant \varepsilon_{sh} \\ f_y + (f_u - f_y)\left(0.4\left(\dfrac{\varepsilon-\varepsilon_{sh}}{\varepsilon_u-\varepsilon_{sh}}\right) + 2\left(\dfrac{\varepsilon-\varepsilon_{sh}}{\varepsilon_u-\varepsilon_{sh}}\right) \Big/ \left(1 + 400\left(\dfrac{\varepsilon-\varepsilon_{sh}}{\varepsilon_u-\varepsilon_{sh}}\right)^5\right)^{1/5}\right) & \text{for } \varepsilon_{sh} \leqslant \varepsilon \leqslant \varepsilon_u \end{cases} \tag{21}$$

The two-stage Ramberg–Osgood material model [61–63] has been found to accurately capture the nonlinear stress–strain response of metallic materials such as cold-formed steels, stainless steels and aluminium alloys. The basic formulation of the two-stage Ramberg–Osgood material model is given by Eq. (22), where the nonlinear stress–strain curve is divided into two stages: below and above the 0.2% proof stress f_y.

$$\varepsilon = \begin{cases} \dfrac{\sigma}{E} + 0.002\left(\dfrac{\sigma}{f_y}\right)^n & \text{for } \sigma \leqslant f_y \\ \dfrac{\sigma - f_y}{E_{0.2}} + \left(\varepsilon_u - \varepsilon_{0.2} - \dfrac{f_u - f_y}{E_{0.2}}\right)\left(\dfrac{\sigma - f_y}{f_u - f_y}\right)^m + \varepsilon_{0.2} & \text{for } f_y < \sigma \leqslant f_u \end{cases} \tag{22}$$

In Eq. (22), $E_{0.2}$ is the tangent modulus of the stress–strain curve at the 0.2% proof stress, which can be defined by Eq. (23), $\varepsilon_{0.2}$ is the total strain at the 0.2% proof stress, equal to $0.002 + f_y/E$, and n and m are the strain hardening exponents, the recommended values of which can be found in Gardner and Yun [61] for cold-formed steels, Afshan et al. [64] and Arrayago et al. [62] for stainless steels and Yun et al. [63] for aluminium alloys.

$$E_{0.2} = \frac{E}{1 + 0.002n\frac{E}{f_y}} \tag{23}$$

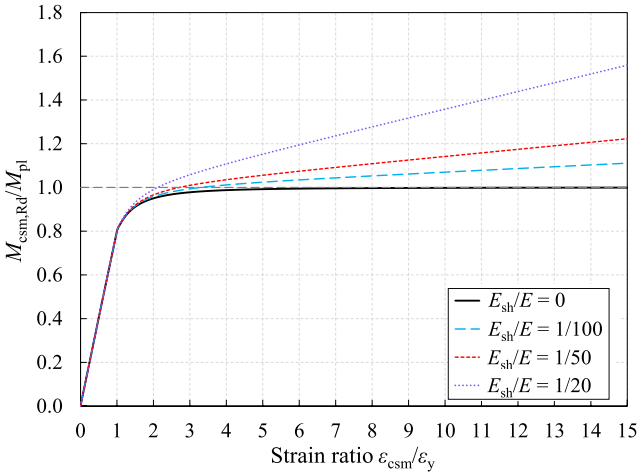

Fig. 7. Variation of normalised CSM bending resistance with strain ratio for materials with rounded stress–strain curves and different strain hardening slopes.

3. CSM cross-section resistance functions

3.1. General

Within the CSM design framework, cross-section resistance is calculated utilising the limiting strain ε_{csm} determined from the CSM base curve, in conjunction with the appropriate CSM material model. The CSM resistance expressions for cross-sections under compression, bending and combined loading are described in the following subsections.

3.2. Compression

The CSM cross-section compression resistance $N_{csm,Rd}$ is determined as the product of the gross cross-section area A and the CSM limiting stress σ_{csm}, as given by:

$$N_{csm,Rd} = \frac{A\sigma_{csm}}{\gamma_{M0}} \tag{24}$$

The CSM limiting stress σ_{csm} is calculated by substituting $\varepsilon = \varepsilon_{csm}$ into the appropriate CSM material model (Eq. (13) or (18)) and determining the corresponding $\sigma = \sigma_{csm}$, and γ_{M0} is the partial safety factor for cross-section resistance; it has been shown that values of 1.0 and 1.1 are suitable for steel [3,59] and stainless steel [7] and aluminium alloy [13,14] design, respectively, allowing the recommended Eurocode values of γ_{M0} to be maintained within the CSM design framework. When $\varepsilon_{csm} > \varepsilon_{sh}$ for hot-rolled steel cross-sections or $\varepsilon_{csm} > \varepsilon_y$ for cold-formed steel, stainless steel and aluminium alloy cross-sections, σ_{csm} will be greater than the yield strength f_y due to the occurrence of strain hardening.

3.3. Bending

For slender cross-sections ($\bar{\lambda}_p > 0.68$ or $\bar{\lambda}_c > 0.3$), the CSM bending resistance $M_{csm,Rd}$ is given simply by the product of the CSM limiting stress σ_{csm} and the elastic section modulus W_{el}, as given by:

$$M_{csm,Rd} = \sigma_{csm}\frac{W_{el}}{\gamma_{M0}} = \frac{\varepsilon_{csm}}{\varepsilon_y}\frac{W_{el}f_y}{\gamma_{M0}} \text{ for } \varepsilon_{csm} \leqslant \varepsilon_y \tag{25}$$

For non-slender hot-rolled steel cross-sections, the CSM bending resistance $M_{csm,Rd}$ depends upon whether or not strain hardening is experienced (i.e. whether or not $\varepsilon_{csm} > \varepsilon_{sh}$). If $\varepsilon_{csm} \leq \varepsilon_{sh}$, the cross-section bending resistance $M_{csm,Rd}$ is given by Eq. (26), where W_{pl} is the plastic section modulus about the axis of bending, and α is a dimensionless coefficient that is equal to 1.2 for I-sections bending about the minor axis and equal to 2 for I-sections bending about the major axis as well as square, rectangular and circular hollow sections (i.e. SHS, RHS and CHS) bending about either principal axis.

$$M_{csm,Rd} = \frac{W_{pl}f_y}{\gamma_{M0}}\left[1 - \left(1 - \frac{W_{el}}{W_{pl}}\right)/\left(\frac{\varepsilon_{csm}}{\varepsilon_y}\right)^{\alpha}\right] \tag{26}$$

for hot-rolled steel cross-sections with $\varepsilon_{csm} \leqslant \varepsilon_{sh}$.

Eq. (26) captures the partial spread of plasticity, resulting in increasing resistance with increasing deformation capacity (i.e. strain ratio $\varepsilon_{csm}/\varepsilon_y$). For stockier hot-rolled steel cross-sections, where $\varepsilon_{csm} > \varepsilon_{sh}$, some benefit from strain hardening can also be exploited, and the CSM cross-section bending resistance is given by Eq. (27):

$$M_{csm,Rd} = \frac{W_{pl}f_y}{\gamma_{M0}}\left[1 - \left(1 - \frac{W_{el}}{W_{pl}}\right)/\left(\frac{\varepsilon_{csm}}{\varepsilon_y}\right)^{\alpha} + \beta\left(\frac{\varepsilon_{csm} - \varepsilon_{sh}}{\varepsilon_y}\right)^2\frac{E_{sh}}{E}\right] \tag{27}$$

for hot-rolled steel cross-sections with $\varepsilon_{csm} > \varepsilon_{sh}$

where β is an additional dimensionless coefficient that is equal to 0.05 for I-sections bending about the minor axis and equal to 0.08 for I-sections bending about the major axis and SHS/RHS bending about either principal axis. A detailed description of the derivation of Eq. (27) can be found in [3].

For non-slender cross-sections made of metallic materials with rounded stress–strain behaviour, the CSM bending resistance $M_{csm,Rd}$ is determined from Eq. (28), which is dependent on the cross-sectional deformation capacity (i.e. strain ratio $\varepsilon_{csm}/\varepsilon_y$) and the strain hardening slope of the material (i.e. E_{sh}). An example of the variation of the normalised CSM bending resistance (i.e. the CSM bending resistance $M_{csm,Rd}$ normalised by the cross-section plastic bending moment M_{pl}) with strain ratio is shown in Fig. 7 for different strain hardening slopes. Bending capacity can be seen to increase smoothly and continuously with increasing deformation capacity, with higher resistances obtained for the materials that exhibit the higher degrees of strain hardening.

$$M_{csm,Rd} = \frac{W_{pl}f_y}{\gamma_{M0}}\left[1 + \frac{E_{sh}}{E}\frac{W_{el}}{W_{pl}}\left(\frac{\varepsilon_{csm}}{\varepsilon_y} - 1\right) - \left(1 - \frac{W_{el}}{W_{pl}}\right)/\left(\frac{\varepsilon_{csm}}{\varepsilon_y}\right)^{\alpha}\right] \tag{28}$$

for cross-sections made of materials with rounded stress-strain behaviour with $\varepsilon_{csm} > \varepsilon_y$.

3.4. Combined loading

The CSM interaction expressions [4] for the design of cross-sections under combined loading are given by Eqs. (29) and (30) for major and minor axis bending plus compression, respectively:

$$M_{y,Ed} \leqslant M_{R,csm,y,Rd} = M_{csm,y,Rd}\left[1 - \left(\frac{N_{Ed}}{N_{csm,Rd}}\right)^{a_y}\right]^{1/b_y} \tag{29}$$

$$M_{z,Ed} \leqslant M_{R,csm,z,Rd} = M_{csm,z,Rd}\left[1 - \left(\frac{N_{Ed}}{N_{csm,Rd}}\right)^{a_z}\right]^{1/b_z} \tag{30}$$

where N_{Ed} is the applied design axial load, M_{Ed} is the applied design bending moment, $N_{csm,Rd}$ and $M_{csm,Rd}$ are the CSM cross-section compression and bending resistances, respectively, $M_{R,csm,Rd}$ is the design CSM bending resistance reduced due to the presence of an axial force N_{Ed} and a_y, a_z, b_y and b_z are dimensionless interaction coefficients that depend on the section type, strain ratio and axis of bending. Note that the suffixes 'y' and 'z' denote bending about the major and the minor axis, respectively.

For biaxial bending plus compression, the following interaction equation applies:

$$\left(\frac{M_{y,Ed}}{M_{R,csm,y,Rd}}\right)^{\alpha_{csm}} + \left(\frac{M_{z,Ed}}{M_{R,csm,z,Rd}}\right)^{\beta_{csm}} \leqslant 1 \tag{31}$$

where α_{csm} and β_{csm} are additional dimensionless interaction coefficients. The interaction coefficients for I-sections, SHS and RHS are defined in Table 2, where a_w and a_f are the ratios of the cross-section web area A_w and flange area A_f to the gross area A, respectively, $W_r = W_{pl,y}/W_{pl,z}$ is the ratio of the major to minor axis plastic section moduli and n_{csm} is the ratio of the design axial load to the CSM cross-section compression resistance N_{Ed}/N_{csm}. Note that all the interaction coefficients are taken equal to unity for strain ratios $\varepsilon_{csm}/\varepsilon_y$ lower than 3, which corresponds to cross-sections with $\bar{\lambda}_p$ values higher than approximately 0.5 (see Fig. 1), resulting in a linear interaction formula for these less stocky cross-sections, as given by Eq. (32).

$$\frac{N_{Ed}}{N_{csm,Rd}} + \frac{M_{y,Ed}}{M_{csm,y,Rd}} + \frac{M_{z,Ed}}{M_{csm,z,Rd}} \leqslant 1 \tag{32}$$

An example of a normalised comparison between collected test and finite element (FE) data for cold-formed steel SHS/RHS under uniaxial bending plus compression [59] with the EN 1993–1-1 [65] interaction curve, with the traditional ends points of the yield load N_y in compression and plastic moment capacity M_{pl} in bending, is shown in Fig. 8. The same data, normalised by the CSM end points, are shown in Fig. 9, alongside the CSM interaction curve [4]. A dramatic improvement in prediction accuracy and reduction in scatter is observed due to the rational exploitation of the spread of plasticity and strain hardening.

It has also been shown that use of the CSM axial and bending resistances as the end points of the existing EN 1993–1-1 [65] interaction curves leads to accurate and consistent strength predictions and improved economy over traditional design methods. This approach has recently been extended to cover the design of stainless steel CHS/SHS/RHS [8–10] and channel sections [11], steel CHS/SHS/RHS [5,54,59] and I-sections [6] and aluminium SHS/RHS [66].

3.5. Non-doubly symmetric cross-sections

For non-doubly symmetric sections in bending, in the case where the neutral axis is closer to the extreme compressive fibre, although the limiting strain in compression may be less than the yield strain, the corresponding strains in tension can be significantly larger than the yield

Table 2
CSM interaction coefficients for cross-sections under combined loading.

	I-sections		SHS and RHS
	$3 \leq \varepsilon_{csm}/\varepsilon_y < 5$	$5 \leq \varepsilon_{csm}/\varepsilon_y \leq 15$	$3 \leq \varepsilon_{csm}/\varepsilon_y \leq 15$
a_y		$a_w + 1.2$	
b_y		0.8	
a_z	2	$8a_w + 1.2$	$a_w + 1.2$
b_z	1	$0.8–0.5a_w$	0.8
α_{csm}	$2 - 1.5n_{csm} \geq 1$	$2 + 0.15W_r - 5n_{csm}^{1.5} \geq 1.3$	$1.75 + W_r(2n_{csm}^2 - 0.15) \leq 1.7 + W_r$
β_{csm}	$0.8 + 5n_{csm}^{2.2} \leq 4$	$0.8 + (15 - W_r)n_{csm}^{2.2} \leq 8$	$1.6 + (3.5 - 1.5W_r)n_{csm}^2 \leq 3.7 - W_r$

strain, resulting in the spread of plasticity and strain hardening. The CSM captures this behaviour by first calculating the limiting strain on the compressive side of the cross-section $\varepsilon_{csm,c}$ from Eq. (1), and then, on the assumption of a linearly-varying through-depth strain distribution and a determined neutral axis position, finding the corresponding strain on the tensile side $\varepsilon_{csm,t}$ [12]. The stress distribution is then derived from the CSM material model. The CSM strain and stress distributions for a T-section, made of materials with rounded stress–strain curves such as stainless steels and aluminium alloys, in major axis bending are shown in Fig. 10. The CSM cross-section bending moment resistance is then determined by integration of the stress distribution throughout the cross-section depth. Simplified design equations for mono-symmetric and asymmetric stainless steel cross-sections in bending have been derived on this basis in [12]. The design approach has been applied to stainless steel angle and channel section beams [67] and aluminium alloy channel section beams [68], and shown to provide accurate and consistent results in comparison to both test and numerical results.

3.6. Improvements in cross-section capacity predictions

The benefits derived from the application of the CSM to the prediction of the resistances of cross-sections of different structural materials have been shown in previous studies [7–14,53,59,60]; for example, average enhancements in capacity over traditional methods of 12% for stainless steel in compression and 19% for stainless steel in bending have been demonstrated [7]. Furthermore, due to the increased consistency and therefore reduction in scatter of the predictions, these enhanced strengths can generally be secured in conjunction with the existing partial safety factors.

4. CSM for steel–concrete composite design

In composite construction, deformation based design enables a more rigorous assessment to be made of the development of the strength of the structural system taking due account of the compatibility between the constituent materials. In this section, recent developments to the deformation based CSM for steel and composite design are described.

Maintaining the basic design philosophy of the CSM, an analytical model to calculate the bending capacity of composite beams with full shear connection under sagging bending moment (see Fig. 11) has been developed [18], allowing for the influence of strain hardening through the quad-linear material model for hot-rolled steels [58] as described in Section 2.3.2. The analytical model for the scenario where the neutral axis lies within the concrete slab, as shown in Fig. 11, and the strain at the bottom outer fibre of the steel section reaches the strain hardening strain ε_{sh}, is outlined herein. The CSM design procedure is as follows:

(1) Determine the neutral axis position $y_{csm,c}$, as shown in Fig. 11, assuming that concrete crushing governs the failure (i.e. the maximum outer fibre strain in the concrete slab reaches the limit of the assumed concrete failure strain of 0.0035) by solving the quadratic Eq. (33).

$$B y_{csm,c}^2 + C y_{csm,c} + D = 0 \tag{33}$$

in which the coefficients B, C and D are given by Eqs. (34)-(36), respectively.

$$B = 0.85 f_{cd} b_{eff} - \frac{0.0035}{2} t_w E_{sh} \left(1 + \frac{\varepsilon_{sh}}{0.0035}\right)^2 \tag{34}$$

$$C = 0.0035 E_{sh} \left(1 + \frac{\varepsilon_{sh}}{0.0035}\right) \left[b_f t_f + t_w (h_c + h_a)\right] - f_y A_a \tag{35}$$

$$D = -0.0035 E_{sh} (h_c + h_a) \left[b_f t_f + \frac{t_w}{2} (h_c + h_a)\right] \tag{36}$$

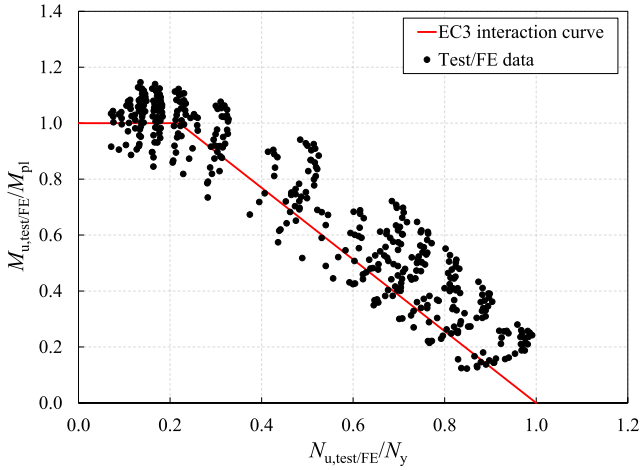

Fig. 8. Capacity comparison between test/FE results and EC3 interaction expression for Class 1 and 2 cold-formed steel SHS/RHS under uniaxial bending plus compression [59].

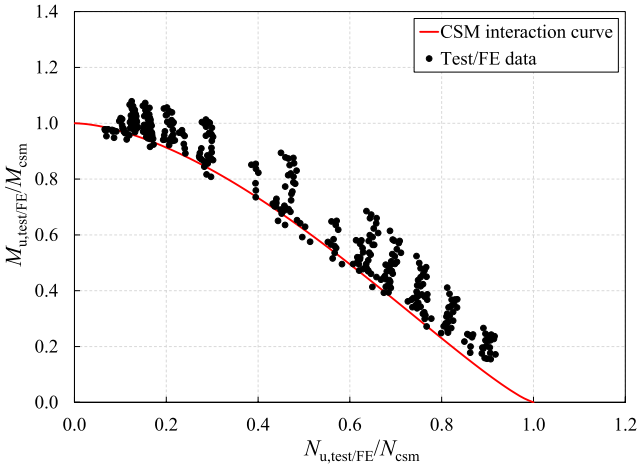

Fig. 9. Capacity comparison between test/FE results and CSM interaction expression for cold-formed steel SHS/RHS with $\bar{\lambda}_p \leqslant 0.5$ under uniaxial bending plus compression [59].

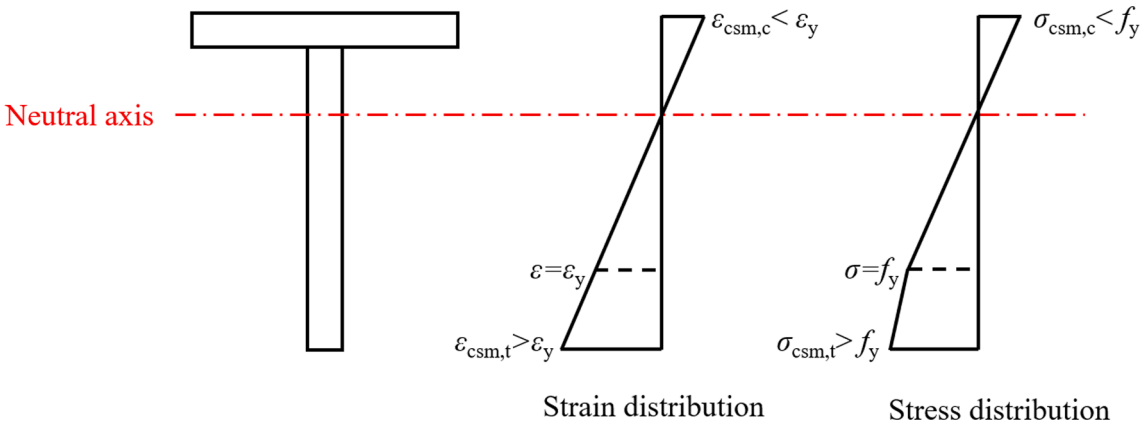

Fig. 10. Application of the CSM to non-doubly symmetric sections subjected to bending.

where f_{cd} is the design concrete (cylinder) compressive strength, b_{eff} is the effective width of the concrete slab, t_w and t_f are the web and flange thickness of the steel beam, respectively, b_f is the flange width of the steel beam, h_a and h_c are the depth of the steel beam and the concrete slab, respectively, and f_y and A_a are the yield strength and cross-sectional area of the steel section, respectively.

(2) Determine the neutral axis position $y_{csm,a}$ assuming that steel failure governs the deformation capacity (i.e. the strain at the outer fibre of the steel section reaches the limiting strain of $15\varepsilon_y$) by Eq. (37).

$$y_{csm,a} = \frac{f_y A_a + E_{sh}\left(15\varepsilon_y - \varepsilon_{sh}\right) b_f t_f + \left(E_{sh}/2\right)\left(15\varepsilon_y - \varepsilon_{sh}\right) t_w \left(h_c + h_a\right)\left(1 - \varepsilon_{sh}/15\varepsilon_y\right)}{0.85 f_{cd} b_{eff} + \left(E_{sh}/2\right)\left(15\varepsilon_y - \varepsilon_{sh}\right) t_w \left(1 - \varepsilon_{sh}/15\varepsilon_y\right)} \tag{37}$$

(3) Calculate the corresponding limiting curvatures $\kappa_{csm,c}$ and $\kappa_{csm,a}$ for concrete failure mode and steel failure mode, respectively:

$$\kappa_{csm,c} = \frac{0.0035}{y_{csm,c}} \tag{38}$$

$$\kappa_{csm,a} = \frac{15\varepsilon_y}{h_c + h_a - y_{csm,a}} \tag{39}$$

The critical curvature κ_{csm} is identified as the lower value of $\kappa_{csm,c}$ and $\kappa_{csm,a}$.

(4) Determine the moment capacity $M_{csm,c,Rd}$ of the composite section using the critical κ_{csm} and its corresponding neutral axis position y_{csm}, as given by Eq. (40).

$$\begin{aligned} M_{csm,c,Rd} = {} & \left(f_{csm} - f_y\right) b_f t_f \left(h_c + h_a - \frac{y_{csm}}{2}\right) + f_y A_a \left(h_c + \frac{h_a}{2} - \frac{y_{csm}}{2}\right) \\ & + \frac{t_w}{12}\left(f_{csm} - f_y\right)\left(h_c + h_a - \frac{\varepsilon_{sh}}{\kappa_{csm}} - y_{csm}\right)\left[4\left(h_c + h_a\right) + 2\frac{\varepsilon_{sh}}{\kappa_{csm}} - y_{csm}\right] \end{aligned} \tag{40}$$

The moment capacities obtained from the developed analytical method have been compared against a series of experimental results collected from the literature on composite beams with full shear connection [18]. The CSM has been shown to provide more accurate predictions of test capacities than the current approach given in EN 1994–1-1 [69], with an average enhancement in resistance of 5% being achieved primarily through the exploitation of strain hardening. For composite beams with partial shear connection, a tentative approach utilising the CSM bending resistance of the bare steel section $M_{csm,Rd}$ (see Eqs. (26) and (27)) and the proposed bending resistance of the composite beam with full shear connection $M_{csm,c,Rd}$ (see Eq. (40)) has been proposed on the basis of numerical investigations [18].

The scope of the CSM for composite structures has been extended in recent research to the design of composite beams under hogging bending moments [19]. Developments to the CSM in the areas of both stainless steel reinforced concrete beams [16,17] and stainless steel–concrete composite beams [20] have also been carried out. Further experimental and analytical research in this area is currently underway.

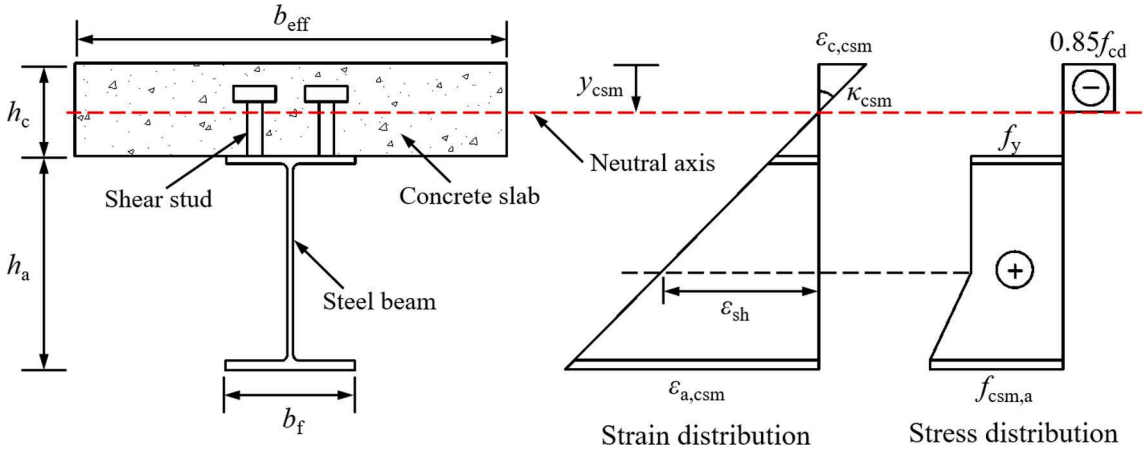

Fig. 11. Strain and stress distribution for a composite beam with full shear connection.

5. Design by advanced inelastic analysis with CSM strain limits

5.1. General

The design of metallic structures is conventionally founded on a two-step process whereby the internal forces and moments are first determined through a simplified structural analysis (e.g. first or second order elastic analysis), then a series of strength and stability checks are carried out on the individual members. For improved design efficiency, system-level advanced analysis, featuring the incorporation of both geometric and material nonlinearities, as well as initial imperfections, can be used. In such an approach, the erosion of stiffness due to buckling and plasticity is explicitly modelled, and consequently the distribution of internal forces and moments within a structure are accurately determined, and frame and member stability effects are directly captured [70]. Advanced structural analysis is commonly carried out using beam finite elements for ease of use and computational efficiency. However, beam finite elements are unable to capture cross-section local buckling behaviour; thus, in current practice (e.g. EN 1993–1-1 [65]), cross-section checks based on the concept of cross-section classification are required. However, the codified treatment of local buckling (i) leads to artificial steps in resistance predictions, (ii) ignores the beneficial effect of strain hardening for compact cross-sections, (iii) fails to accurately account for the spread of plasticity in Class 3 (semi-compact) sections and (iv) fails to capture the beneficial effect of bending moment gradients along member lengths on local cross-section stability. Additionally, classification is based upon the most slender plate element within the cross-section thereby neglecting the beneficial interaction between the individual plate elements of the cross-section during local buckling. With the aim of overcoming these drawbacks resulting from the concept of cross-section classification, a more consistent design approach has been developed [29–34], whereby the CSM strain limits are used to simulate the influence of local buckling in a second order inelastic analysis using beam elements. This method has been included in AISC 370 [40] for stainless steel design and is due for inclusion in prEN 1993–1-14 [38] for hot-rolled steel, cold-formed steel and stainless steel design. The key aspects of the design method are summarised in Section 5.2, while two illustrative examples are provided in Section 5.3.

5.2. Key aspects of design by advanced inelastic analysis with CSM strain limits

In this design approach, beam elements are employed to perform an advanced inelastic analysis, i.e. a geometrically and materially nonlinear analysis with imperfections (GMNIA). The ultimate resistance of a member or structure is then determined from the GMNIA as the first to occur of (1) the load at which the average strain across the cross-section elastic local buckling half-wavelength (described later) reaches the corresponding CSM limit strain, or (2) the peak load, after which the load–deformation response decreases. The full material stress–strain behaviour i.e. sharply defined yielding for hot-rolled steel [58] and a rounded response for cold-formed steel [61], stainless steel [62,64] and aluminium [63] should be appropriately modelled, and account should be taken for both initial geometric imperfections and residual stresses. Residual stresses can either be introduced explicitly or through equivalent bow imperfections that allow for the combined effects of geometric imperfections and residual stresses. Equivalent bow imperfections for design by GMNIA have been derived for flexural buckling [71], lateral-torsional buckling [72] and combined loading [73] and are included in prEN 1993–1-14 [38].

The CSM strain limits should be applied to all cross-sections in the structure, and are determined using the CSM base curve, given by Eqs. (1) and (2) when a material model with a sharply-defined yield point (e.g. hot-rolled steel) is used, and Eqs. (41) and (42) when a rounded material model (e.g. the two-stage Ramberg–Osgood model for cold-formed steels, stainless steels and aluminium alloys) is used, where σ is the maximum compressive stress [29]. The latter CSM base curve equations compensate for the 0.2% strain offset that was subtracted from the cold-formed steel, stainless steel and aluminium data in the derivation of the CSM base curve and material model (see Section 2.3.2).

$$\frac{\varepsilon_{csm}}{\varepsilon_y} = \frac{0.25}{\bar{\lambda}_p^{3.6}} + \frac{0.002}{\varepsilon_y} \text{ but } \frac{\varepsilon_{csm}}{\varepsilon_y} \leqslant \Omega, \text{ for } \bar{\lambda}_p \leqslant 0.68 \tag{41}$$

$$\frac{\varepsilon_{csm}}{\varepsilon_y} = \left(1 - \frac{0.222}{\bar{\lambda}_p^{1.05}}\right)\frac{1}{\bar{\lambda}_p^{1.05}} + \frac{0.002\left(\sigma/f_y\right)^n}{\varepsilon_y}, \text{ for } 0.68 < \bar{\lambda}_p \leqslant 1.0 \tag{42}$$

The beneficial effect of strain gradients (generally resulting from local moment gradients) on the local stability of cross-sections, i.e. the ability of the less heavily loaded cross-sections to provide some support in resisting local buckling to the adjacent critical cross-section, have been previously recognised [74–76]. To account for this beneficial effect, a strain averaging approach has been developed and implemented into design by advanced analysis [29–34]. The strain averaging approach requires the CSM strain limit ε_{csm} to be applied to an averaged compressive strain $\varepsilon_{Ed,Lb}$ across the local buckling half-wavelength $L_{b,cs}$ (see Fig. 12) rather than the maximum compressive strain along the length of a member. The elastic local buckling half-wavelength $L_{b,cs}$ can be obtained numerically e.g. using the finite strip method software

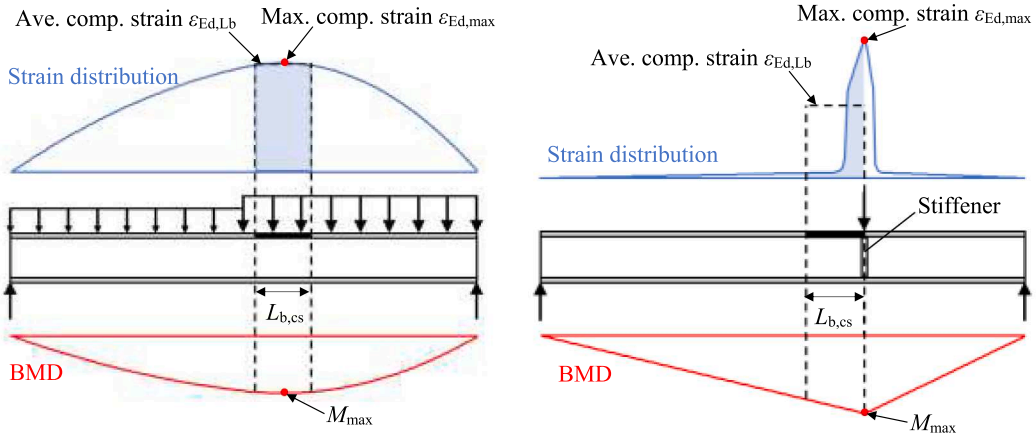

(a) Beam without stiffeners (b) Compact section beam (experiencing high strains)

Fig. 12. Bending moment diagrams (BMD), strain distributions and typical locations of $L_{b,cs}$ for (a) a beam without web stiffeners and (b) a beam with a web stiffener.

CUFSM [43] or through explicit formulae [77] based on the first order internal force distribution. All cross-sections must be checked; however, the critical cross-section is often easy to identify, e.g. that subjected to the highest bending moment M_{max}, as shown in Fig. 12(a). For structural members with stiffeners, local buckling is constrained within the vicinity of the stiffener and hence $L_{b,cs}$ is located to either side of the stiffener; typically the side with the shallower moment gradient will govern (see Fig. 12(b)) [30]. Note that in the calculation of the averaged strain $\varepsilon_{Ed,Lb}$, only the beam elements that lie wholly within the averaging length $L_{b,cs}$ should be considered.

In cases of high shear force and/or torsion, allowance needs to be made to account for the adverse influence on the bending capacity. In this design method, the influence of the interaction between bending, shear and torsion is accounted for by applying a reduced strain limit $\varepsilon_{csm,V}$ [30,34]. As an example, for I-sections under combined bending and shear, the reduced strain limit $\varepsilon_{csm,V}$ is given by Eq. (43), where ρ_y and ρ_z are the reduction factors ranging from 0 to 1.0 to allow for the influence of high vertical and lateral shear, as given by Eqs. (44) and (45), respectively, $\mu_{y,fl}$ is given by Eq. (46) and $\mu_{z,w}$ is the ratio of the cross-section minor axis bending moment resistance determined neglecting the presence of the flanges M_w to the elastic minor axis bending resistance of the full cross-section $M_{el,z}$. Note that $\mu_{z,w}$ is negligible for I-sections since $M_w \approx 0$.

$$\varepsilon_{csm,V} = \varepsilon_{csm} - \rho_y\left(\varepsilon_{csm} - \mu_{y,fl}\varepsilon_y\right) - \rho_z\left(\varepsilon_{csm} - \mu_{z,w}\varepsilon_y\right) \tag{43}$$

$$\rho_y = \begin{cases} 0 & \text{for } \dfrac{V_{y,Ed}}{V_{y,Rk}} \leqslant 0.5 \\ \left(\dfrac{2V_{y,Ed}}{V_{y,Rk}} - 1\right)^2 & \text{for } \dfrac{V_{y,Ed}}{V_{y,Rk}} > 0.5 \end{cases} \tag{44}$$

$$\rho_z = \begin{cases} 0 & \text{for } \dfrac{V_{z,Ed}}{V_{z,Rk}} \leqslant 0.25 \\ 1 - \sqrt{1 - \left(\dfrac{V_{z,Ed}}{V_{z,Rk}}\right)^2} & \text{for } 0.25 < \dfrac{V_{z,Ed}}{V_{z,Rk}} < 1.0 \\ 1 & \text{for } \dfrac{V_{z,Ed}}{V_{z,Rk}} = 1.0 \end{cases} \tag{45}$$

where $V_{y,Ed}$ and $V_{z,Ed}$ are the design value of shear forces and $V_{y,Rk}$ and $V_{z,Rk}$ are the cross-section shear resistances, taken as the plastic cross-section shear resistances.

$$\mu_{y,fl} = \frac{bt_f\left(h - t_f\right)f_y}{M_{el,y}} \tag{46}$$

Note that separate cross-section shear capacity and shear buckling checks are also required, which can be carried out using the relevant provisions of EN 1993–1-1 [65] and EN 1993–1-5 [51].

An overview of how the key structural phenomenon are treated in the described design method i.e. design by GMNIA with CSM strain limits and the traditional design methods provided in EN 1993–1-1 [65] for steel members and frames has been presented by Fieber et al. [31] and is summarised in Table 3. The comparisons highlight the advantages of using the advanced CSM-based design approach, with a more

Table 3
Overview of treatment of key structural phenomena in EN 1993–1-1 [65] and design by GMNIA with CSM strain limits [30].

	Design method						
	EN 1993–1-1 [65]						GMNIA using beam elements with CSM strain limits
	Elastic design			Plastic design			
Global analysis*	LA	GNA	GNIA	MNA	GMNA	GMNIA	GMNIA
Frame imperfections	Imperfect geometry or equivalent horizontal forces (EHF)			Imperfect geometry or equivalent horizontal forces (EHF)			Imperfect geometry or equivalent horizontal forces (EHF)
Member imperfections	Member buckling checks		Equivalent imperfections	Member buckling checks		Equivalent imperfections	Equivalent imperfections
Local imperfection and local buckling	Cross-section classification; effective width method for Class 4 cross-sections			Cross-section classification; plastic analysis limited to structures with Class 1 cross-sections			Strain limits
P - Δ effects (frame buckling)	Ignored if $\alpha_{cr} \geq 10$; Otherwise approx. methods		Global analysis	Ignored if $\alpha_{cr} \geq 15$; Otherwise approx. methods		Global analysis	Global analysis
P - δ effects (member buckling)	Member buckling checks		Global analysis + cross-section checks	Member buckling checks		Global analysis	Global analysis
Moment gradient effect on member stability	Member buckling checks with C_m factors		Global analysis	Member buckling checks with C_m factors		Global analysis	Global analysis
Moment gradient effect on local stability	Ignored			Ignored			Strain averaging approach
Force/moment redistribution due to member buckling	Ignored		Captured in global analysis	Ignored		Captured in global analysis	Captured in global analysis
Force/moment redistribution due to material yielding	Ignored			Captured in global analysis			Captured in global analysis and controlled by CSM strain limits
Spread of plasticity	Ignored in analysis, approximated in design checks for Class 1 and 2 cross-sections			Captured in global analysis using elastic, perfectly plastic material model			Captured in global analysis and controlled by CSM strain limits
Strain hardening	Ignored			Ignored			Material model with strain hardening

*Different analysis types: (i) linear elastic analysis (LA), (ii) geometrically nonlinear analysis (GNA), (iii) geometrically nonlinear analysis with imperfections (GNIA), (iv) first order materially nonlinear analysis (MNA), (v) geometrically and materially nonlinear analysis (GMNA), (vi) geometrically and materially nonlinear analysis with imperfections (GMNIA).

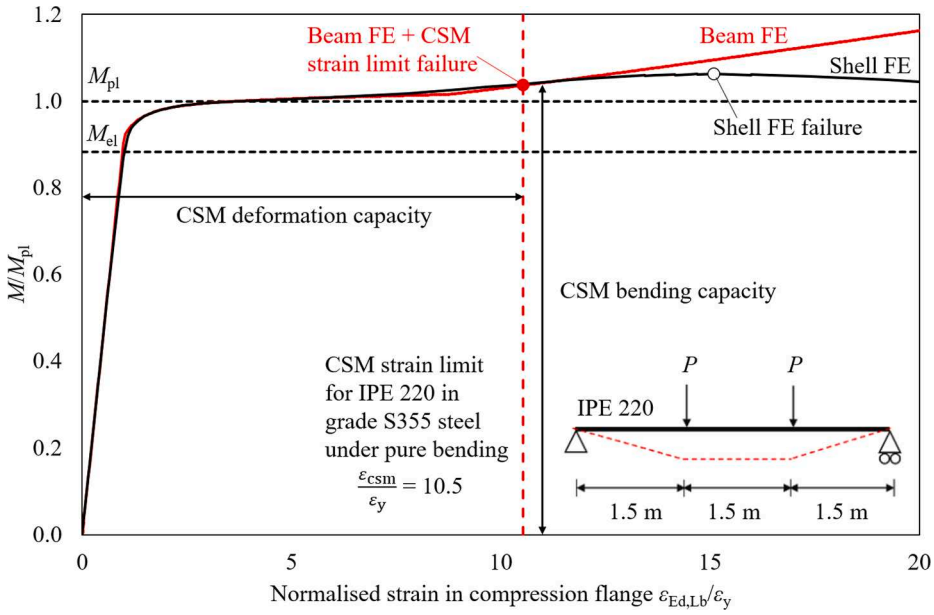

Fig. 13. Illustrative example of design by GMNIA with CSM strain limits on a simply-supported IPE 220 S355 steel beam subjected to four-point bending.

consistent, rational and systematic treatment of local buckling, material nonlinearity, strain hardening and the influence of local moment gradients. This has been further demonstrated in a number of studies [29,30,32–34] showing that design by GMNIA with CSM strain limits enables accurate predictions of the resistance of structures while allowing for the structural failure mechanism to be clearly visualised. More details on the treatment of the interaction between bending, shear and torsion and some key aspects of the FE modelling in the framework of design by GMNIA can be found in [30,34].

5.3. *Illustrative examples*

In this subsection, the application of the method of design by GMNIA with CSM strain limits is illustrated with reference to a simply-supported hot-rolled steel beam subjected to four-point bending and a two-span stainless steel continuous beam.

5.3.1. *Hot-rolled steel I-section beam*

Fig. 13 presents the normalised moment-strain responses of a 4.5 m simply-supported IPE 220 beam subjected to four-point bending obtained from shell and beam FE models. Note that in the FE models, only

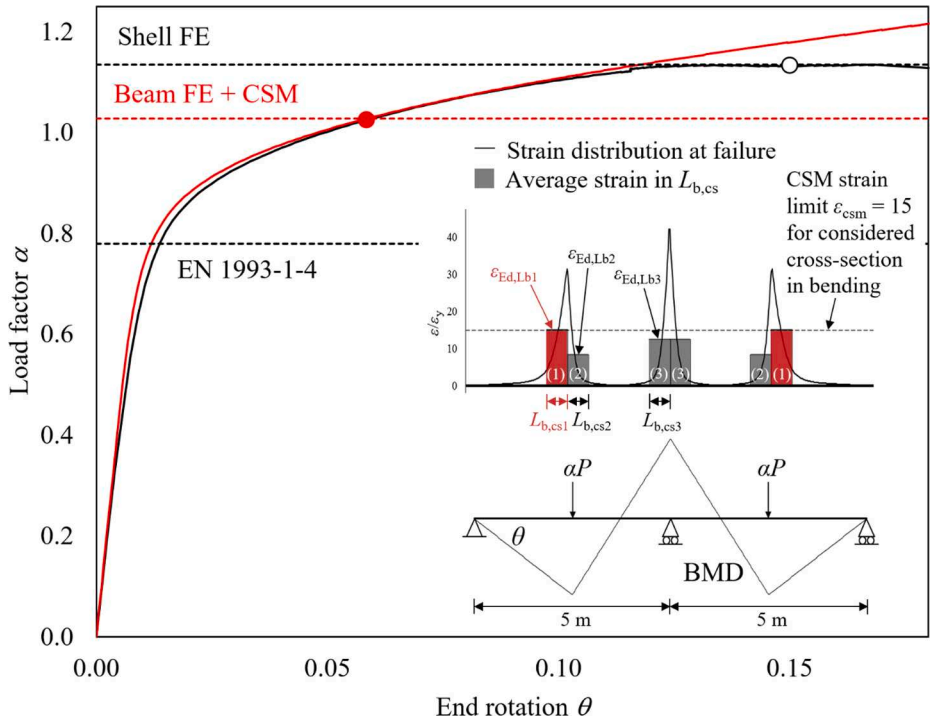

Fig. 14. Illustrative example of design by GMNIA with CSM strain limits on a two-span austenitic stainless steel continuous beam subjected to mid-span point loads [29].

in-plane behaviour is considered and out-of-plane restraints were provided to prevent lateral-torsional buckling. As shown in Fig. 13, the benchmark shell FE model undergoes a degree of plasticity and strain hardening before reaching a peak bending moment of $M_{u,shell} = 1.06M_{pl}$. Failure, caused by inelastic local buckling of the compression flange at the critical cross-section is explicitly captured by the shell FE model. The beam FE model, on the other hand, is unable to capture cross-section failure and hence no peak load arises in the GMNIA. However, cross-section failure is accounted for in the developed design method through the application of the CSM strain limit, with failure defined as the point at which the average compressive strain at any cross-section in the system reaches the CSM strain limit. Note that, in the present example, there is uniform bending moment in the critical mid-span region of the beam; hence, there are no moment gradient effects, and the average compressive strain $\varepsilon_{Ed,Lb}$ across the critical local buckling half-wavelength is the same as the maximum compressive strain at the critical cross-section. The normalised CSM strain limit $\varepsilon_{csm}/\varepsilon_y$ for an IPE 220 made of grade S355 steel under pure bending is 10.5 (calculated using Eq. (1), where the cross-section slenderness $\bar{\lambda}_p = 0.35$, based on an elastic critical buckling stress of $\sigma_{cr,cs} = 2837$ MPa, calculated using the formulae given in [45]). Application of this strain limit to the beam element GMNIA results in a resistance prediction $M_{u,beam} = 1.04M_{pl}$, which is close but on the safe side of the shell FE model prediction, while providing a 4% increase in capacity over the EN 1993–1-1 [65] resistance prediction of M_{pl}.

5.3.2. Stainless steel I-section continuous beam

With increasing indeterminacy, which is typically associated with more complex structural systems, the benefits of performing design by GMNIA with CSM strain limits tend to increase; while at member level, the CSM strain limits capture the beneficial effects of the spread of plasticity, strain hardening and local moment gradients, at system level, the strain limits also control the degree of permissible moment redistribution due to plastification and instability. In traditional design, the permitted level of plastic moment redistribution is very crudely determined based on the classification of the cross-section – in structures composed of Class 1 cross-sections, full moment redistribution is allowed, while for Class 2 (or higher) cross-sections, no moment redistribution is allowed.

Fig. 14 shows the load-end rotation responses of a two-span

Table 4
State of Continuous Strength Method development.

Topic	Details	Research Status			Reference
		Existing	Ongoing	Needed	
Material modelling	Hot-rolled steel	✓			[58]
	Cold-formed steel	✓			[59]
	Stainless steel	✓			[7,60]
	Aluminium	✓			[13,63]
	High strength steel	✓		✓	[58,61]
	Elevated temperature	✓		✓	[23]
CSM for cross-section design	SHS/RHS under compression/bending/combined loading	✓			[1–5,7,9,10,13,14,60,66,79–82]
	CHS/EHS[1]/SOHS[2]/FOHS[3] under compression/bending/combined loading	✓		✓	[8,53,79–86]
	I-/Channel/Angle/T-sections under compression/bending/combined loading	✓		✓	[3,6,11,12,67,68,87–92]
	Additively manufactured cross-sections under compression/bending/combined loading	✓	✓	✓	[93,94]
	Slender cross-sections under compression/bending/combined loading	✓		✓	[53,79,80,95–97]
	Cross-sections in shear or torsion	✓		✓	[98–100]
	Stiffened cross-sections	✓		✓	[101]
	Perforated cross-sections	✓	✓	✓	[100,102–105]
	Cross-sections under concentrated transverse load		✓	✓	
CSM for member design	Flexural buckling of SHS/RHS columns	✓	✓	✓	[25,106,107]
	CHS/SHS/RHS/I-section Beam-columns	✓	✓	✓	[26,28,108–110]
	Lateral/Lateral-torsional buckling of uniform/tapered structural components	✓	✓	✓	[24]
	Distortional buckling e.g. for lipped channels			✓	
CSM for composite design	Composite beams under sagging bending moment	✓			[18]
	Composite beams under hogging bending moment	✓			[19]
	CFRP-strengthened concrete-filled stainless steel tubular stub columns	✓		✓	[21]
	Steel-reinforced concrete beams	✓	✓	✓	[16,17]
	Concrete-filled steel tubular elements	✓	✓	✓	[111,112]
	Bamboo composite tubes	✓	✓	✓	[113]
CSM for design by advanced analysis	SHS/RHS/I-section structural members under compression/bending/combined loading	✓		✓	[29,30,34]
	Continuous beams/frames with I-section or SHS/RHS profiles	✓		✓	[31,32,114–117]
	Flexural/lateral-torsional buckling of web-tapered steel I-section members	✓	✓	✓	[33]
	Advanced analysis to high strength/stainless steel frames made of tapered/uniform members		✓	✓	
CSM for connections	Aluminium/stainless steel *T*-stubs	✓	✓	✓	[15,119]
	Stainless steel staggered bolted connections in tension	✓	✓	✓	[120]
CSM for fire design	Cross-sections under compression/bending	✓		✓	[22,118]
	Cross-sections under combined loading	✓		✓	[23]
	Beam-columns		✓	✓	
	Lateral/lateral-torsional buckling of uniform/tapered structural components			✓	
CSM for seismic design	Cold-formed stainless steel RHS beams	✓	✓	✓	[121]
	Seismic design of cross-sections, members and systems			✓	

Table notes: 1. EHS = elliptical hollow sections. 2. SOHS = semi-oval hollow sections. 3. FOHS = flat-oval hollow sections.

austenitic stainless steel W14×82 continuous beam obtained from shell and beam FE models. Note that in the FE models, only in-plane behaviour is considered and out-of-plane restraints were provided to prevent lateral-torsional buckling. The bending moment and normalised maximum compressive strain distributions at failure determined from the beam FE GMNIA are also shown in Fig. 14. The considered W14×82 cross-section has a local buckling half-wavelength $L_{b,cs}$ equal to 500 mm (determined from the finite strip software CUFSM [43]), a cross-section slenderness $\bar{\lambda}_p$ equal to 0.31 (determined from the finite strip software CUFSM [43]) and a corresponding CSM strain limit $\varepsilon_{csm}/\varepsilon_y$ of 15 (determined from the CSM base curve, see Eq. (32)).

It can be seen from the normalised maximum compressive strain distribution that there are three potential failure regions, $L_{b,cs1}$, $L_{b,cs2}$ and $L_{b,cs3}$, within each span of the continuous beam, with the length of each potential failure region equal to the local buckling half-wavelength of 500 mm. The average compressive strains at failure across the three potential failure regions, $\varepsilon_{Ed,Lb,1}$, $\varepsilon_{Ed,Lb,2}$ and $\varepsilon_{Ed,Lb,3}$, are also shown in Fig. 14. It is observed that while the peak strain occurs at the location of the internal support (i.e. $L_{b,cs3}$), the moment gradient is very steep (and hence beneficial) at this point. The critical cross-section is found to arise at the location of the point loads (i.e. $L_{b,cs1}$), where the peak strain is lower, but the moment gradient is shallower and hence less beneficial. This critical location corresponds to the point of failure observed in the corresponding shell FE model. Design by GMNIA using beam elements with the CSM strain limit $\varepsilon_{csm}/\varepsilon_y = 15$ for this continuous beam results in a system resistance prediction that is close to but on the safe side of the shell FE model prediction, while providing a 32% increase in capacity over EN 1993–1-4 [78]. Design by second order inelastic analysis allows the structural failure mechanism to be accurately captured and visualised, and has been shown to provide consistent capacity predictions for a wide range of steel and stainless steel members and structural systems [29–34].

6. Summary and outlook

6.1. Summary of CSM development

A summary of the current state of developments of the CSM is presented in Table 4. The CSM developments are categorised into seven major groups: material modelling, design of cross-sections, design of members, design of composite structures, design by advanced analysis, connection design, fire design and seismic design. The status of each different research topic is described in Table 4 as existing, ongoing or needed, depending on whether the research topic has been addressed in the literature, is known to the authors as being conducted or is considered to be important for further development, respectively. In addition, the most relevant references for each topic are selected and provided in Table 4 for interested readers.

6.2. Outlook

Although extensive research has been carried out on the development and expansion of the CSM for steel and steel-composite design, there remains a number of areas where further research is required, as identified in Table 4. Selected topics are described in this section to provide researchers with a view on what is needed for further development of the CSM.

Accurate constitutive modelling is a key feature of any advanced analysis or design method, including the CSM. Material models for hot-rolled steel [58], cold-formed steel [61], stainless steel [62,64] and aluminium [63] have been established based on extensive datasets of experimental stress–strain curves collected from the literature. However, there are only a relatively limited number of tensile coupon test results on high strength steel reported in the literature; thus additional test data on high strength steel are required to verify and potentially improve current models. Further experimental data are also needed at elevated temperatures and high strain rates [122].

The CSM design of non-slender cross-sections has been systematically studied, while the design method for slender cross-sections, considering the influence of element interaction on post-local buckling behaviour, merits further investigation. Moreover, despite some existing research on cross-sections in shear [98], a systematic study on cross-sections under combined shear and bending is lacking. Significant work also remains to be done on extending the CSM to the design of cross-sections under concentrated transverse loads, as well as cross-sections manufactured using new techniques, such as wire arc additive manufacturing [123,124].

Research into the application of the CSM to the design of members has shown significant promise in the case of stainless steel [25,26]. Further studies are required to extend the initial research to members of different cross-section types and materials. Other buckling modes, including distortional buckling, lateral-torsional buckling and torsional-flexural buckling also require attention.

Extension of the CSM to the design of concrete-filled steel tubular (CFST) members has been explored [125], but requires further research. Compared with empty steel tubular sections, local buckling is inhibited in concrete-filled specimens due to the presence of the concrete. By allowing for the influence of the concrete infill on the local buckling stress and hence slenderness of the steel section, the CSM failure strain of the steel tube can be obtained from the base curve. This can be used to assess compatibility with the concrete failure strain, predict the failure mode and hence determine the resistance of the composite cross-section. Strain-based design of CFST members is considered to be a topic with substantial potential for research and impact on practice. Composite construction featuring other combinations of materials, such as steel and timber [126] is also considered to be an area of fruitful research, including the establishment of CSM-based design criteria.

A number of researchers have explored the CSM design of indeterminate structures [31,32,114–117], including through design by GMNIA using beam elements with CSM strain limits [29–34]. Design by GMNIA with CSM strain limits has been extensively verified for continuous beams and plane frames made of normal strength steel and stainless steel but requires further research for three-dimensional frames, trusses, structures at elevated temperatures and under seismic loading, as well as composite structures and structures composed of different materials.

Work performed in [15,118,120] demonstrates the possibility to extend the CSM to the design of steel connections. For connections made of hardening materials, the ultimate bending moment resistances of the plastic hinges can substantially exceed their plastic bending moments. Through application of the CSM to determine the ultimate resistance of hardening plastic hinges, the accuracy of resistance predictions can be significantly improved through the explicit consideration of strain compatibility and hence the rational exploitation of the spread of plasticity and strain hardening. Further work is needed in this area.

A number of studies into the development and assessment of the CSM for the design of steel cross-sections at elevated temperatures [22,23,118] have been carried out. Further research is required to extend the CSM to cover steel cross-sections subjected to thermal gradients and steel members at elevated temperatures. The potential to use the CSM to consider combinations of mechanical and thermal loading through a rational strain-based approach should be explored. Application of the CSM to structures composed of other materials should also be investigated. In addition to fire, another extreme loading condition is that corresponding to seismic actions, where the importance of ductility and failure mode control [127,128] is well known. Owing to its explicit consideration of deformations, there is potential for the CSM to be expanded to consider cross-section failure under an accumulation of plastic strains, thereby predicting the structural response and ultimately inelastic local buckling and fracture from low cycle fatigue; an initial study presented in [121] shows promising results.

Finally, work is needed in developing authoritative supporting guidance documents, worked examples and training on the CSM, to promote its wider use among designers and manufacturers. Overall, although the CSM now features in a number of international design standards, as outlined in this section, there remains considerable scope for refinement, development and expansion with the aim to bring greater efficiency to structural design, thus leading to more sustainable construction.

7. Conclusions

The Continuous Strength Method (CSM) is a deformation-based structural design approach in which cross-section failure is defined based on strain limits. A review of the background, development and current status of the CSM has been presented herein. The CSM allows for a rational exploitation of the spread of plasticity, strain hardening and moment redistribution. The limiting strain that a cross-section can endure is determined, as a function of cross-section slenderness, from the CSM base curve; this replaces the notion of cross-section classification. The limiting strain is then used in conjunction with simplified CSM material models, the strain hardening modulus of which varies to reflect the degree of strain hardening of the considered material (i.e. hot-rolled steel, cold-formed steel, stainless steel or aluminium), to determine the cross-section resistance under the applied loading conditions – compression, bending or combined loading. Application of the CSM is performed through straightforward hand calculations, and significant benefits in terms of accuracy of resistance predictions and reduction in scatter are achieved. In addition to the design of conventional metal structural elements, the CSM has been applied to connection design, composite structures, structures in fire and reinforced concrete structures. The strain based design approach has also been integrated into the framework of design by advanced analysis (GMNIA), where more sophisticated material models are used, and yet further benefits arise.

The CSM has been formally adopted in the North American and European design codes for stainless steel structures [35–37,39,40] and in the new Eurocode (EN 1993–1-14) for the design of steel structures by finite element analysis [38]. Further developments to the CSM are ongoing and, although much has been achieved, there remains considerable scope for further research and wider application in practice.

Declaration of Competing Interest

The authors declare that they have no known competing financial interests or personal relationships that could have appeared to influence the work reported in this paper.

Data availability

Data will be made available on request.

References

[1] Gardner L. A new approach to structural stainless steel design. PhD thesis, Department of Civil and Environmental Engineering, Imperial College London, UK; 2002.
[2] Gardner L. The continuous strength method. Proc Inst Civ Eng: Struct Build 2008; 161(3):127–33.
[3] Yun X, Gardner L, Boissonnade N. The continuous strength method for the design of hot-rolled steel cross-sections. Eng Struct 2018;157:179–91.
[4] Liew A, Gardner L. Ultimate capacity of structural steel cross-sections under compression, bending and combined loading. Structures 2015;1:2–11.
[5] Yun X, Wang ZX, Gardner L. Structural performance and design of hot-rolled steel SHS and RHS under combined axial compression and bending. Structures 2020; 21:1289–98.
[6] Yun X, Gardner L, Boissonnade N. Ultimate capacity of I-sections under combined loading–Part 2: Parametric studies and CSM design. J Constr Steel Res 2018;148: 265–74.
[7] Afshan S, Gardner L. The continuous strength method for structural stainless steel design. Thin-Walled Struct 2013;68:42–9.
[8] Zhao O, Gardner L, Young B. Structural performance of stainless steel circular hollow sections under combined axial load and bending–Part 2: Parametric studies and design. Thin-Walled Struct 2016;101:240–8.
[9] Arrayago I, Real E. Experimental study on ferritic stainless steel RHS and SHS cross-sectional resistance under combined loading. Structures 2015;4:69–79.
[10] Zhao O, Rossi B, Gardner L, Young B. Experimental and numerical studies of ferritic stainless steel tubular cross sections under combined compression and bending. J Struct Eng ASCE 2016;142(2):04015110.
[11] Liang Y, Zhao O, Long YL, Gardner L. Stainless steel channel sections under combined compression and minor axis bending–Part 2: Parametric studies and design. J Constr Steel Res 2019;152:162–72.
[12] Zhao O, Gardner L. The continuous strength method for the design of mono-symmetric and asymmetric stainless steel cross-sections in bending. J Constr Steel Res 2018;150:141–52.
[13] Su MN, Young B, Gardner L. The continuous strength method for the design of aluminium alloy structural elements. Eng Struct 2016;122:338–48.
[14] Su MN, Young B, Gardner L. Testing and design of aluminum alloy cross-sections in compression. J Struct Eng ASCE 2014;140(9):04014047.
[15] Wang Z, Wang Y, Zhang Y, Gardner L, Ouyang Y. Experimental investigation and design of extruded aluminium alloy T-stubs connected by swage-locking pins. Eng Struct 2019;200:109675.
[16] Rabi M, Cashell KA, Shamass RJ. Flexural analysis and design of stainless steel reinforced concrete beams. Eng Struct 2019;198:109432.
[17] Rabi M, Cashell KA, Shamass RJ. Ultimate behaviour and serviceability analysis of stainless steel reinforced concrete beams. Eng Struct 2021;248:113259.
[18] Gardner L, Yun X, Macorini L, Kucukler M. Hot-rolled steel and steel-concrete composite design incorporating strain hardening. Structures 2017;9:21–8.
[19] Yang F, Liu Y, Xin H. Negative bending capacity prediction of composite girders based on continuous strength method. Thin-Walled Struct 2018;129:278–88.
[20] Shamass R, Cashell KA. Analysis of stainless steel-concrete composite beams. J Constr Steel Res 2019;152:132–42.
[21] Sharif AM, Al-Mekhlafi GM, Al-Osta MA. Structural performance of CFRP-strengthened concrete-filled stainless steel tubular short columns. Eng Struct 2019;183:94–109.
[22] Theofanous M, Prospert T, Knobloch M, Gardner L. The continuous strength method for steel cross-section design at elevated temperatures. Thin-Walled Struct 2016;98:94–102.
[23] Yun X, Saari N, Gardner L. Behaviour and design of eccentrically loaded hot-rolled steel SHS and RHS stub columns at elevated temperatures. Thin-Walled Struct 2020;149:106646.
[24] Anwar-Us-Saadat M, Ashraf M. The continuous strength method for lateral-torsional buckling of stainless steel I-beams. Thin-Walled Struct 2018;130: 148–60.
[25] Arrayago I, Real E, Mirambell E, Gardner L. The Continuous Strength Method for the design of stainless steel hollow section columns. Thin-Walled Struct 2020; 154:106825.
[26] Arrayago I, Real E, Mirambell E, Gardner L. The Continuous Strength Method for the design of stainless steel hollow section beam-columns. Eng Struct 2021;238: 111981.
[27] Tse K, Wang J, Yun X. Structural behaviour and continuous strength method design of high strength steel non-slender welded I-section beam-columns. Thin-Walled Struct 2021;169:108273.
[28] Yun X, Meng X, Gardner L. Design of cold-formed steel SHS and RHS beam-columns considering the influence of steel grade. Thin-Walled Struct 2022;171: 108600.
[29] Walport F, Gardner L, Nethercot DA. Design of structural stainless steel members by second order inelastic analysis with CSM strain limits. Thin-Walled Struct 2021;159:107267.
[30] Fieber A, Gardner L, Macorini L. Design of structural steel members by advanced inelastic analysis with strain limits. Eng Struct 2019;199:109624.
[31] Fieber A, Gardner L, Macorini L. Structural steel design using second-order inelastic analysis with strain limits. J Constr Steel Res 2020;168:105980.
[32] Gardner L, Yun X, Fieber A, Macorini L. Steel design by advanced analysis: material modeling and strain limits. Engineering 2019;5(2):243–9.
[33] Quan C, Kucukler M, Gardner L. Design of web-tapered steel I-section members by second-order inelastic analysis with strain limits. Eng Struct 2020;224:111242.
[34] Quan C, Kucukler M, Gardner L. Out-of-plane stability design of steel beams by second-order inelastic analysis with strain limits. Thin-Walled Struct 2021;169: 108352.
[35] AISC Design guide 27: Structural stainless steel. American Institute of Steel Construction (AISC); 2013.
[36] SCI Design manual for structural stainless steel, 4th edition. The Steel Construction Institute (SCI), UK; 2017.
[37] prEN 1993-1-4. Eurocode 3: Design of steel structures – Part 1-4: General rules – Supplementary rules for stainless steels. Draft 2. Brussels: European Committee for Standardization (CEN); 2020.
[38] prEN 1993-1-14. Eurocode 3: Design of steel structures – Part 1-14: Design assisted by finite element analysis. Brussels: European Committee for Standardization (CEN); 2021.
[39] ASCE-8-21: Specification for the Design of Cold-Formed Stainless Steel Structural Members. Draft for public review. The American Society of Civil Engineers (ASCE); 2021.
[40] AISC. 370: Specification for Structural Stainless Steel Buildings. Draft for public review. The American Institute of Steel Construction (AISC); 2021.
[41] Schafer BW. The direct strength method of cold-formed steel member design. J Constr Steel Res 2008;64(7–8):766–78.

[42] Schafer BW. Advances in the Direct Strength Method of cold-formed steel design. Thin-Walled Struct 2019;140:533–41.
[43] Schafer BW, Ádány S. Buckling analysis of cold-formed steel members using CUFSM: conventional and constrained finite strip methods. Proceedings of the 18th International Specialty Conference on Cold-Formed Steel Structures, 26-27 October 2006, Orlando, Florida, USA, 39-54.
[44] Seif M, Schafer BW. Local buckling of structural steel shapes. J Constr Steel Res 2010;66(10):1232–47.
[45] Gardner L, Fieber A, Macorini L. Formulae for calculating elastic local buckling stresses of full structural cross-sections. Structures 2019;17:2–20.
[46] Gardner L, Ashraf M. Structural design for non-linear metallic materials. Eng Struct 2006;28(6):926–34.
[47] Ashraf M, Gardner L, Nethercot DA. Structural stainless steel design: resistance based on deformation capacity. J Struct Eng ASCE 2008;134(3):402–11.
[48] Bruneau M, Uang CM, Whittaker A. Ductile design of steel structures. McGraw-Hill; 1998.
[49] Ricles JM, Sause R, Green PS. High-strength steel: implications of material and geometric characteristics on inelastic flexural behavior. Eng Struct 1998;20(4–6):323–35.
[50] Kuhlmann U. Definition of flange slenderness limits on the basis of rotation capacity values. J Constr Steel Res 1989;14:21–40.
[51] EN 1993-1-5. Eurocode 3: Design of steel structures – Part 1-5: Plated structure elements. Brussels: European Committee for Standardization (CEN); 2006.
[52] Gardner L, Nethercot DA. Structural stainless steel design: a new approach. Struct Eng 2004;82:21–30.
[53] Buchanan C, Gardner L, Liew A. The continuous strength method for the design of circular hollow sections. J Constr Steel Res 2016;118:207–16.
[54] Meng X, Toffolon A, Gardner L, Taras A. The generalized slenderness-based resistance method for the design of CHS and EHS. Steel Constr 2019;12(4):342–53.
[55] Donnell LH. A new theory for the buckling of thin cylinders under axial compression and bending. Trans ASME 1934;56:795–806.
[56] Rotter JM, Sadowski AJ, Chen L. Nonlinear stability of thin elastic cylinders of different length under global bending. Int J Solids Struct 2014;51(15–16):2826–39.
[57] Chan TM, Gardner L, Law KH. Structural design of elliptical hollow sections: a review. Proc Inst Civ Eng: Struct Build 2010;165(6):391–402.
[58] Yun X, Gardner L. Stress-strain curves for hot-rolled steels. J Constr Steel Res 2017;133:36–46.
[59] Yun X, Gardner L. The continuous strength method for the design of cold-formed steel non-slender tubular cross-sections. Eng Struct 2018;175:549–64.
[60] Bock M, Gardner L, Real E. Material and local buckling response of ferritic stainless steel sections. Thin-Walled Struct 2015;89:131–41.
[61] Gardner L, Yun X. Description of stress-strain curves for cold-formed steels. Constr Build Mater 2018;189:527–38.
[62] Arrayago I, Real E, Gardner L. Description of stress-strain curves for stainless steel alloys. Mater Des 2015;87:540–52.
[63] Yun X, Wang ZX, Gardner L. Full-range stress–strain curves for aluminum alloys. J Struct Eng ASCE 2021;147(6):04021060.
[64] Afshan S, Zhao O, Gardner L. Standardised material properties for numerical parametric studies of stainless steel structures and buckling curves for tubular columns. J Constr Steel Res 2019;152:2–11.
[65] EN 1993-1-1. Eurocode 3: Design of steel structures — Part 1–1: General rules and rules for buildings. Brussels: European Committee for Standardization (CEN); 2005.
[66] Bock M, Theofanous M, Dirar S, Lipitkas N. Aluminium SHS and RHS subjected to biaxial bending: Experimental testing, modelling and design recommendations. Eng Struct 2021;227:111468.
[67] Zhang L, Tan KH, Zhao O. Local stability of press-braked stainless steel angle and channel sections: Testing, numerical modelling and design analysis. Eng Struct 2020;203:109869.
[68] Zhu JH, Li ZQ, Su M, Young B. Design of aluminum alloy channel section beams. J Struct Eng ASCE 2020;146(5):04020074.
[69] EN 1994-1-1. Eurocode 4: Design of composite steel and concrete structures – Part 1-1: General rules and rules for buildings. Brussels: European Committee for Standardization (CEN); 2005.
[70] Walport F, Gardner L, Nethercot DA. A method for the treatment of second order effects in plastically-designed steel frames. Eng Struct 2019;200:109516.
[71] Walport F, Gardner L, Nethercot DA. Equivalent bow imperfections for use in design by second order inelastic analysis. Structures 2020;26:670–85.
[72] Quan C, Walport F, Gardner L. Equivalent imperfections for the out-of-plane stability design of steel beams by second-order inelastic analysis. Eng Struct 2022;251:113481.
[73] Quan C, Walport F, Gardner L. Equivalent imperfections for the design of beam-columns by second-order inelastic analysis. (In submission).
[74] Lay MG, Galambos TV. The inelastic behavior of beams under moment gradient. Fritz Engineering Laboratory Report No. 297.12, Lehigh University, 1964.
[75] Wang J, Afshan S, Gkantou M, Theofanous M, Baniotopoulos C, Gardner L. Flexural behaviour of hot-finished high strength steel square and rectangular hollow sections. J Constr Steel Res 2016;121:97–109.
[76] Saloumi E, Hayeck M, Nseir J, Boissonnade N. Slenderness-based design criteria to allow for the plastic analysis of tubular beams. J Constr Steel Res 2019;105788.
[77] Fieber A, Gardner L, Macorini L. Formulae for determining elastic local buckling half-wavelengths of structural steel cross-sections. J Constr Steel Res 2019;159:493–506.
[78] EN 1993-1-4. Eurocode 3: Design of steel structures – Part 1-4: General rules – Supplementary rules for stainless steels. Brussels: European Committee for Standardization (CEN); 2006.
[79] Lan X, Chen J, Chan TM, Young B. The continuous strength method for the design of high strength steel tubular sections in compression. Eng Struct 2018;162:177–87.
[80] Lan X, Chen J, Chan TM, Young B. The continuous strength method for the design of high strength steel tubular sections in bending. J Constr Steel Res 2019;160:499–509.
[81] Zhang Y, Liu Y, Sheng R, Dong X, Yang F. Cross-sectional moment capacity prediction of steel box girders based on the CSM. J Bridge Eng 2022;27(7):04022051.
[82] Li B, Wang Y, Zhang Y, Yuan H, Zhi X, Baniotopoulos CC. Flexural behaviour of 7A04-T6 high-strength aluminium alloy SHS and RHS beams under moment gradient. Eng Struct 2022;259:114138.
[83] Chen MT, Young B. Behavior of cold-formed steel elliptical hollow sections subjected to bending. J Constr Steel Res 2019;158:317–30.
[84] Chen MT, Young B. Material properties and structural behavior of cold-formed steel elliptical hollow section stub columns. Thin-Walled Struct 2019;134:111–26.
[85] Chen MT, Young B. Cross-sectional behavior of cold-formed steel semi-oval hollow sections. Eng Struct 2018;177:318–30.
[86] Sachidananda K, Singh KD. Numerical study of fixed ended lean duplex stainless steel (LDSS) flat oval hollow stub column under pure axial compression. Thin-Walled Struct 2015;96:105–19.
[87] Yuan HX, Wang YQ, Shi YJ, Gardner L. Stub column tests on stainless steel built-up sections. Thin-Walled Struct 2014;83:103–14.
[88] da S Sirqueira A, da S Vellasco PCG, de Lima LRO, Sarquis FR. Experimental assessment of stainless steel hot-rolled equal legs angles in compression. J Constr Steel Res 2020;169;106069.
[89] Zhu JH, Li ZQ, Su MN, Young B. Behaviour of aluminium alloy plain and lipped channel columns. Thin-Walled Struct 2019;135:306–16.
[90] Chen S, Fang H, Liu JZ, Chan TM. Design for local buckling behaviour of welded high strength steel I-sections under bending. Thin-Walled Struct 2022;172:108792.
[91] Liu JZ, Chen S, Chan TM. Experimental and numerical investigations of hybrid high strength steel welded T-section stub columns with Q690 flange and Q460 web. Thin-Walled Struct 2022;177:109403.
[92] Georgantzia E, Gkantou M, Kamaris GS, Kansara KD. Design of aluminium alloy channel sections under minor axis bending. Thin-Walled Struct 2022;174:109098.
[93] Buchanan C, Matilainen VP, Salminen A, Gardner L. Structural performance of additive manufactured metallic material and cross-sections. J Constr Steel Res 2017;136:35–48.
[94] Zhang R, Gardner L, Buchanan C, Matilainen VP, Piili H, Salminen A. Testing and analysis of additively manufactured stainless steel CHS in compression. Thin-Walled Struct 2021;159:107270.
[95] Zhao O, Afshan S, Gardner L. Structural response and continuous strength method design of slender stainless steel cross-sections. Eng Struct 2017;140:14–25.
[96] Ahmed S, Ashraf M, Anwar-Us-Saadat M. The continuous strength method for slender stainless steel cross-sections. Thin-Walled Struct 2016;107:362–76.
[97] Anwar-Us-Saadat M, Ashraf M, Ahmed S. Behaviour and design of stainless steel slender cross-sections subjected to combined loading. Thin-Walled Struct 2016;104:225–37.
[98] Saliba NG, Gardner L. Deformation-based design of stainless steel cross-sections in shear. Thin-Walled Struct 2018;123:324–32.
[99] Devi SV, Singh KD. The continuous strength method for circular hollow sections in torsion. Eng Struct 2021;242:112567.
[100] Devi SV, Singh KD. Finite element study of lean duplex stainless steel semi-elliptical hollow section members with circular perforation subjected to torsion. Thin-Walled Struct 2020;146:106464.
[101] Su MN, Young B, Gardner L. Flexural response of aluminium alloy SHS and RHS with internal stiffeners. Eng Struct 2016;121:170–80.
[102] Feng R, Zhan H, Meng S, Zhu J. Experiments on H-shaped high-strength steel beams with perforated web. Eng Struct 2018;177:374–94.
[103] Lepcha KH, Patton ML. A numerical study on structural behaviour of lean duplex stainless steel tubular beams with rectangular web openings. Structures 2021;32:1233–49.
[104] Feng R, Sun W, Shen C, Zhu J. Experimental investigation of aluminum square and rectangular beams with circular perforations. Eng Struct 2017;151:613–32.
[105] Wang L, Hu M, Young B. Tests of aluminum alloy perforated built-up sections subjected to bending. Thin-Walled Struct 2021;158:107136.
[106] Ahmed S, Ashraf M. Numerical investigation on buckling resistance of stainless steel hollow members. J Constr Steel Res 2017;136:193–203.
[107] Tuezney S, Lauwens K, Afshan S, Rossi B. Buckling of stainless steel welded I-section columns. Eng Struct 2021;236:111815.
[108] Yang L, Zhao M, Gardner L, Ning K, Wang J. Member stability of stainless steel welded I-section beam-columns. J Constr Steel Res 2019;155:33–45.
[109] Bu Y, Gardner L. Laser-welded stainless steel I-section beam-columns: Testing, simulation and design. Eng Struct 2019;179:23–36.
[110] Buchanan C, Zhao O, Real E, Gardner L. Cold-formed stainless steel CHS beam-columns–Testing, simulation and design. Eng Struct 2020;213:110270.
[111] Dai P, Yang L, Wang J, Ning K, Gang Y. Compressive behavior of concrete-filled square stainless steel tube stub columns. Steel Compos Struct 2022;42(1):91–106.

[112] Elsisy AR, Shao YB, Zhou M, Hassanein MF. A study on the compressive strengths of stiffened and unstiffened concrete-filled austenitic stainless steel tubular short columns. Ocean Eng 2022;248:110793.
[113] Wei Y, Chen S, Tang S, Zheng K, Wang J. Mechanical behavior of bamboo composite tubes under axial compression. Constr Build Mater 2022;339:127681.
[114] Su MN, Young B, Gardner L. Continuous beams of aluminum alloy tubular cross sections. II: parametric study and design. J Struct Eng ASCE 2015;141(9): 04014233.
[115] Arrayago I, Real E, Mirambell E. Design of stainless steel continuous beams with tubular cross-sections. Eng Struct 2017;151:422–31.
[116] Gkantou M, Kokosis G, Theofanous M, Dirar S. Plastic design of stainless steel continuous beams. J Constr Steel Res 2019;152:68–80.
[117] Yun X, Gardner L. Numerical modelling and design of hot-rolled and cold-formed steel continuous beams with tubular cross-sections. Thin-Walled Struct 2018;132: 574–84.
[118] Su MN, Zhang Y, Young B. Design of aluminium alloy beams at elevated temperatures. Thin-Walled Struct 2019;140:506–15.
[119] Yuan HX, Hu S, Du XX, Yang L, Cheng XY, Theofanous M. Experimental behaviour of stainless steel bolted T-stub connections under monotonic loading. J Constr Steel Res 2019;152:213–24.
[120] dos Santos JJ, Liang Y, Zhao O, de Andrade SAL, de Lima LRO, Gardner L, et al. Testing and design of stainless steel staggered bolted connections. Eng Struct 2021;231(111707).
[121] Gonzalez-de-Leon I, Arrayago I, Real E, Nastri E. Rotation capacity of cold-formed stainless steel RHS beams under cyclic loading. J Constr Steel Res 2022;192: 107199.
[122] Yang X, Yang H, Gardner L, Wang Y. A continuous dynamic constitutive model for normal- and high-strength structural steels. J Constr Steel Res 2022;192:107254.
[123] Kanyilmaz A, Demir AG, Chierici M, Berto F, Gardner L, Kandukuri SY, et al. Role of metal 3D printing to increase quality and resource-efficiency in the construction sector. Addit Manuf 2022;50:102541.
[124] Huang C, Kyvelou P, Zhang R, Britton TB, Gardner L. Mechanical testing and microstructural analysis of wire arc additively manufactured steels. Mater Des 2022;216:110544.
[125] Lam D, Gardner L. Structural design of stainless steel concrete filled columns. J Constr Steel Res 2008;64(11):1275–82.
[126] Kyvelou P, Gardner L, Nethercot DA. Testing and analysis of composite cold-formed steel-wood-based flooring systems. J Struct Eng ASCE 2017;143(11): 04017146.
[127] Uang CM, Bruneau M, Whittaker AS, Tsai KC. Seismic Design of Steel Structures. In: Naeim, F. (eds) The Seismic Design Handbook 2001; Springer, Boston, MA.
[128] Xu F, Chan TM, Sheehan T, Gardner L. Prediction of ductile fracture for circular hollow section bracing members under extremely low cycle fatigue. Eng Struct 2020;214:110579.